

**Dielectric Function and Plasmonic Excitation on Hydrogen
Terminated Diamond Surface**

Submitted by

Xinxin Peng

Bachelor of Science, 2013 NUA

Master of Science, 2016 NUA

**A thesis submitted in total fulfilment
of the requirements for the degree of
Master of Science**

**Department of Chemistry and Physics
School of Molecular Sciences
College of Science, Health and Engineering**

**La Trobe University
Victoria, Australia**

August 2020

Abstract


Plasmonic excitation involves the coupling of electromagnetic wave and oscillation of surface charge carriers, which is promising for the application in optical communication, bio-sensing, lab-on-chip, etc. The plasmonic excitation has been realized on a variety of two-dimensional materials such as graphene and some transition metal dichalcogenide monolayers (TMDC) materials, but it still remains unknown whether the quasi-two-dimensional (Q2D) hole gas formed on the hydrogen terminated diamond can support propagating plasmons. In this thesis to investigate such problems in relating to the dielectric function, I introduced triangular well instead of the commonly used square potential for a model Q2D system, representing a more realistic description of the surface confining potential. We found that plasmon energy is proportional to the square root of wavenumber when it is small, and proportional to the square of wavenumber when it exceeds $10^9 m^{-1}$. The plasmon frequency needed for excitation for the Q2D system of hole gas on hydrogen-terminated diamond was subsequently predicted to be around 2 GHz. The theoretical framework developed in this work in obtaining the dielectric function for a Q2D system with a non-square confining potential will not only guide future experimental work in this field but also lay a foundation to model the realistic dielectric functions in other types of promising 2D or Q2D materials.

The preliminary measurements of photocurrent and ellipsometry were also conducted on diamond, which shows that the wavelength relevant to photoconductivity occurs in 500 nm visible light regime, and there is slight difference between the dielectric functions of hydrogen and oxygen terminated diamond. Future directions can include verifying whether plasmonic response of the diamond by terahertz or far-infrared light can be coupled to the photocurrent effect, and whether the higher signal to noise ratio generated by forming 2D hole gas on a much thinner diamond substrate would give us a different result in ellipsometry.

Statement of Authorship

This thesis includes work by the author that has been published or accepted for publication as described in the text. Except where reference is made in the text of the thesis, this thesis contains no other material published elsewhere or extracted in whole or in part from a thesis accepted for the award of any other degree or diploma. No other person's work has been used without due acknowledgment in the main text of the thesis.

This thesis has not been submitted for the award of any degree or diploma in any other tertiary institution.

Signed, 

Xinxin Peng

10 June 2020

Acknowledgement

First I would like to thank my supervisor and mentor, Dr. Shanshan Kou. Her great support and invaluable advice in all situations helped me to progress through my work since the first year I moved to Melbourne. Your guidance, patience and instruction helped me immensely through my study, and I will be constantly inspired by your passion in exploring the unknown when doing research.

I have had a number of co-supervisors and research progress panel members who have been keeping my study on track; to Dr. Dongchen Qi, your knowledge in material science has kept reminding me of the importance of how theoretical study should be interpreted from the perspective of experimentalists. I have learned so much since the beginning of my PhD from our discussions and under your guidance. To Dr. David Hoxley, thank you for offering me your insight in the area of diamond. I benefitted a lot from the advices you have given in writing this thesis. To Dr. Brian Abbey and Prof. Narelle Brack, thanks for your work in looking after all the research progress panel meetings, I feel so supported in this journey. And to Prof. Lothar Ley, though I am not officially your student, I have been so privileged to get your guidance in this area. And your prudence and humbleness will always be the beacon in my life.

To all other people at La Trobe university that I worked with. Particularly, Kaijian Xing and Lei Zhang (who visited La Trobe from NUS) for encouragement, motivation and offering great advice along the way. To Dr. Arif Siddiquee, Panji Achmari, Steve Yianni, Hugh Marman and Susannah Holmes, working alongside you have been a lot fun and comforting.

I would also like to extend a special thanks to FOCUS (Fellowship of Overseas Christian University Students) at La Trobe Uni, where I have made lots of friends who have given me the strength and endurance to finish the degree in the time of stress and uncertainty. To Sally Boyd, thanks for your help in polishing the grammatical errors in this thesis and your wisdom in handling stress. I will not be able to list all the names of friends I met there, but the support and friendship you have given me are deeply cherished in my heart.

This work was supported by a La Trobe University Postgraduate Research Scholarship and a La Trobe University Full Fee Research Scholarship.

Contents

| | |
|--|-----|
| List of Figures | vii |
| Acronyms, abbreviations and conventions | ix |
| 1 Introduction | 1 |
| 2 Literature review | 4 |
| 2.1 Fundamentals of plasmonics | 4 |
| 2.1.1 History of studies into surface plasmon polariton | 4 |
| 2.1.2 Overview of surface plasmon plasmon | 5 |
| 2.1.3 Two-dimensional material nanophotonics | 11 |
| 2.2 Theoretical models of plasmons in quasi-two-dimensional systems | 15 |
| 2.2.1 Self-consistent approach to obtain dielectric function | 16 |
| 2.2.2 Calculation of the dielectric function within quasi-2D system | 18 |
| 2.3 Optical explorations for plasmonic dielectric functions on two-dimensional materials | 21 |
| 2.3.1 Ellipsometry measurement | 21 |
| 2.3.2 Scanning near-field optical microscopy | 23 |
| 3 Dielectric function and plasmon dispersion relation of a quasi-two-dimensional hole gas on hydrogen terminated diamond surface | 27 |
| 3.1 Introduction | 27 |
| 3.2 Model of a confined hole gas | 29 |
| 3.3 Calculation of dielectric function of Q2D hole gas | 31 |
| 3.3.1 Solving to obtain induced potential | 32 |
| 3.3.2 Dispersion relation of the collective excitation of a Q2D system | 34 |
| 3.3.3 Comparison of static dielectric function between Q2D and 2D system | 37 |
| 3.3.4 Conclusions | 39 |
| 4 Future work | 41 |
| 4.1 Introduction | 41 |
| 4.2 Measurement of photoconductivity of hydrogen-terminated diamond | 41 |
| 4.3 Ellipsometry measurements | 45 |
| 4.4 Refinement on theoretical analysis | 46 |
| 5 Summary and Conclusion | 48 |
| References | 49 |

List of Figures

| | |
|---|----|
| 1.1: Application of plasmonics: Bio-communication, lab-on-chip and molecular sensing..... | 1 |
| 2.1: Schematic illustration of electromagnetic wave and surface charges at the interface between the metal and the dielectric material..... | 7 |
| 2.2: Dispersion relations for light wave, bulk plasmons, surface plasmons, surface plasmon polariton and 2D plasmons..... | 9 |
| 2.3: Two ways to excite plasmon..... | 10 |
| 2.4: Schematic setup of an ellipsometry experiment..... | 21 |
| 2.5: Different types of scanning near-field optical..... | 23 |
| 2.6: Functional schematics of the SNOM measuring head..... | 24 |
| 2.7: Schematic of SNOM measurement for probing plasmon on graphene..... | 26 |
| 3.1: Schematic picture of the hydrogenated diamond surface doped by water..... | 28 |
| 3.2: Two dimensional hole dispersion relation in a triangular well for carriers whose density is 10^{13} cm^{-2} | 30 |
| 3.3: Plasmon dispersion relation for 2D and Q2D systems of different effective electric strength..... | 35 |
| 3.4: Dispersion relation for photon and Q2D system without external electric field..... | 36 |
| 3.5: Form factor γ and F_{1111} as a function of q | 37 |
| 3.6: Static dielectric function is shown as a function for Q2D and 2D systems and also for Thomas-Fermi approximation..... | 38 |
| 4.1: Schematic image of the device design for photocurrent measurement..... | 42 |
| 4.2: The relation between photoconductance and wavelength in the hydrogenated area..... | 43 |
| 4.3: The comparison of I-V measurements in dark and with 525 nm laser illumination for oxygen-terminated channel..... | 44 |

| | |
|---|----|
| 4.4: Dielectric function of hydrogen and oxygen terminated diamond in the infrared range..... | 45 |
|---|----|

Acronyms, abbreviations and conventions

2D/3D: two/ three dimensional

Q2D: quasi-two-dimensional

2DHG: two dimensional hole gas

SPP: surface plasmon polariton

SNOM: scanning near-field optical microscopy

LPSR: localized surface plasmon resonance

TMDC: transition metal dichalcogenide monolayers

EM: electromagnetic

TM: transverse magnetic

TE: transverse electric

ω : frequency

q : wavenumber

DFT: density functional theory

Introduction

Plasmonics refers to a discipline for utilizing the resonant interaction between electromagnetic radiation (light) and free charge carriers at the interface between a metal and a dielectric material (e.g. air or glass). It serves as the technique to merge photonics and electronics at nanoscale dimensions, thus the strengths of these two areas can be combined for the application in optical communication, bio-sensing, lab-on-chip, etc. (Fig (1.1)). The development of plasmonics has led to remarkable fundamental insights into the interaction between light and matter at the nanoscale, which allow the diffraction limit [1] to be crossed and novel imaging techniques to be created like the scanning near-field optical microscopy (SNOM) [2], and paves the way to enable two-dimensional (2D) materials with extraordinary optical properties that don't often exist in the nature.

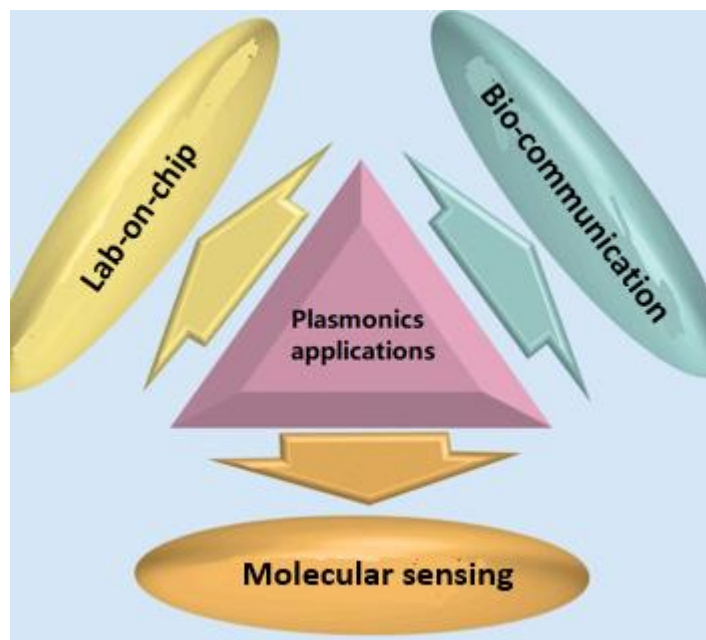


Figure 1.1 Application of plasmonics: Bio-communication, lab-on-chip and molecular sensing.

In exploring the plasmonic effect, dielectric function is the key parameter in determining optoelectronic properties. In macroscopic scale, it relates an electric field \mathbf{E} to the induced

dielectric polarization density \mathbf{P} , and in general is a 3×3 Cartesian tensor unless the dielectric is homogenous. Whereas in the microscopic scale, the derivation is based on how the system reacts to an external electric force. Since the response is dependent on frequency and wave vector, dielectric function is also a function of frequency and wave vector. Bulk plasmon dispersion relation, which is essentially the relation between plasmon frequency and its wave vector, is obtained after setting the dielectric function to be zero. Whereas surface plasmon is more depending on the relation of dielectric function of the interface separating metal and dielectric material. 2D/quasi-2D (Q2D) plasmon can be viewed as the bulk plasmon in the lower dimension, which exhibits lots of fascinating properties, such as tunability via modulating the gate voltage, and integrability to all kinds of electronic devices [3].

Most of the studies of 2D or surface plasmonics focus on the coupling of free electrons to light in metals or 2D materials like graphene, less attention has been devoted to the 2D hole system. Hydrogen terminated diamond stands out due to its being transparent in the visible wavelength range, high thermal conductivity, and extremely high hardness. A 2D hole gas layer can be formed on the bulk diamond after pristine diamond being exposed to high temperature hydrogen plasmon [4], therefore the dielectric-conductive layer structure makes it a perfect candidate for plasmonic excitation. The main work of this thesis is the derivation of dielectric function and plasmonic dispersion relation of 2D hole gas on the hydrogen terminated diamond surface. The main work of this thesis is the derivation of dielectric function and plasmonic dispersion relation of the 2D hole gas on the hydrogen terminated diamond surface.

The thesis is organised as follows:

In Chapter 2 the plasmonic effect and the methods to derive the dielectric function of 2D/Q2D materials are reviewed. First the history of studies into surface plasmon polariton are given, which is followed by the discussion of the 2D plasmon. Afterwards self-consistent approach to obtain dielectric function in Q2D system are reviewed in detail, which prepares for the extension into the case of hydrogen terminated diamond surface. Then experimental techniques to investigate the optical properties are introduced, such as ellipsometry and scanning near-field optical microscopy (SNOM).

Chapter 3 gives the main results utilising a self-consistent field approach on hydrogen terminated diamond with a triangular confining potential representing the band profile at the surface. Derivations of its dielectric and plasmonic properties are demonstrated, which include the dielectric function, the plasmonic dispersion relation and static dielectric function.

In the fourth chapter, future work on the optoelectronic properties of hydrogen terminated diamond are explored, including its photoconductivity and ellipsometry measurement. These early explorations can provide directions towards plasmonic excitation on the hydrogen terminated diamond surface.

In the final chapter, a summary of the whole thesis is given with indications of potential applications of this work.

2

Literature review

2.1 Fundamentals of plasmonics

In this literature review, fundamentals of plasmonics are firstly. Afterwards the comparison between the surface plasmon polariton and two-dimensional (2D) plasmon are introduced. To get the dispersion relation of plasmon, one needs to know the dielectric function of certain material. Therefore the theoretical model of deriving dielectric function in 2D/quasi-2D is discussed in second section. In last section, various experimental methods to investigate the plasmonic effect, including ellipsometry and scanning near-field microscopy (SNOM), are reviewed.

2.1.1 History of studies into surface plasmon polariton

Surface plasmon polaritons are often referred to under the topic of plasmonics. To obtain an overview of surface plasmon polariton and to clarify the meaning and the origin of different related terms such as plasmons and polaritons, the evolution of the term surface plasmon polariton (SPP) will be introduced in the following chronological order.

The study of surface plasmon polariton started more than one century ago when Zenneck *et.al.* [5] in year 1907 and Sommerfeld *et.al.* [6] in year 1909 firstly reported that when emitting electromagnetic waves impinge onto a planar or spherical boundary interface between two media with different dielectric function, the surface electromagnetic waves propagate parallel to the interface, and decay exponentially vertical to it.

Later on K.B. Tolpygo [7] in 1950 and K. Huang [8] in 1951 discussed the coupling of electromagnetic waves and phonons in ionic crystals, and the coupling was called polariton by John Hopfield [9] afterwards. Furthermore, D. Bohm *et.al.* [10] in 1953 explained the energy losses of fast electrons passing through metal foil by oscillation of electrons in a

metallic solid, and they called this phenomena excitation plasmons.

Whereafter H Frohlich *et. al.* [11] in 1955 showed that there existed longitudinal electric plasma oscillations in silver films when dielectric function equals zero, and the plasma oscillation is accepted by the scientific community as the name of plasmons nowadays. In 1957 Ritchie [12] first proposed the prediction that new lowered loss of energy compared to the loss caused by bulk plasmons is due to the boundary effect, and he called the surface collective oscillations *surface plasmons* in his paper. SPP came into realization in 1968 by A. Otto [13] utilising the method of frustrated total reflection, in which the surface plasma wave is coupled with photon thus forming a new kind of propagating wave.

Overall plasmon reflects the intrinsic collective properties of the material (normally metal or semi-conductor), while polariton is the coupling of plasmon with propagating electromagnetic waves [14].

2.1.2 Overview of surface plasmon plasmon

Plasmonics is the study of the interactions between an electromagnetic field and the free charge carriers (usually electrons) in a conductive medium. The wave-like movement of free electrons can have a well-defined wavelength, which is related to their momentum $p = \hbar k$ [14]. In the case of plasmons within conductive materials, namely bulk plasmons, electrons are shifted in the presence of an external force caused by an electric field. However, when electrons are displaced, positive charges are left behind, which exert an attractive force on the displaced particles pulling them back to their original positions. This Coulombic restoring force makes the electrons oscillate back and forth like a simple harmonic oscillator.

The bulk plasmon frequency can be expressed by Eq. 2.1 solving the simple harmonic motion equation. In this expression, the terms n , e , m_{eff} , ϵ_0 and ω_p represent: conduction electron density, electron charge, effective mass of the electron, dielectric function in free space, and plasmon frequency, respectively [14]

$$\omega_p = \sqrt{\frac{ne^2}{m_{eff}\epsilon_0}} \quad (2.1)$$

The plasmonic oscillations can also occur at the interface between a metal and a dielectric material. These oscillations at the interface are referred to as surface plasmons (SPs), which are essentially two-dimensional (2D) electron oscillations along the interface of the two materials [14], and the strong coupling of electromagnetic (EM) waves with surface plasmons is referred to as SPP. While for Localized Surface Plasmon Resonance (LSPR), another branch of plasmonics, it can be seen as the non-propagating version of SPP. LSPR happens in the interfaces of noble metal particles and dielectric, here the size of noble metal particles is comparable to or smaller than the wavelength of incident light. Thus the plasmon effect is confined to the particle surface and is highly sensitive to the refractive index of the dielectric.

One way to obtain the dispersion relation is to solve the Maxwell Equations providing the boundary conditions [14], while the other is utilizing the Fresnel reflection coefficient which is repeated in detail here [15].

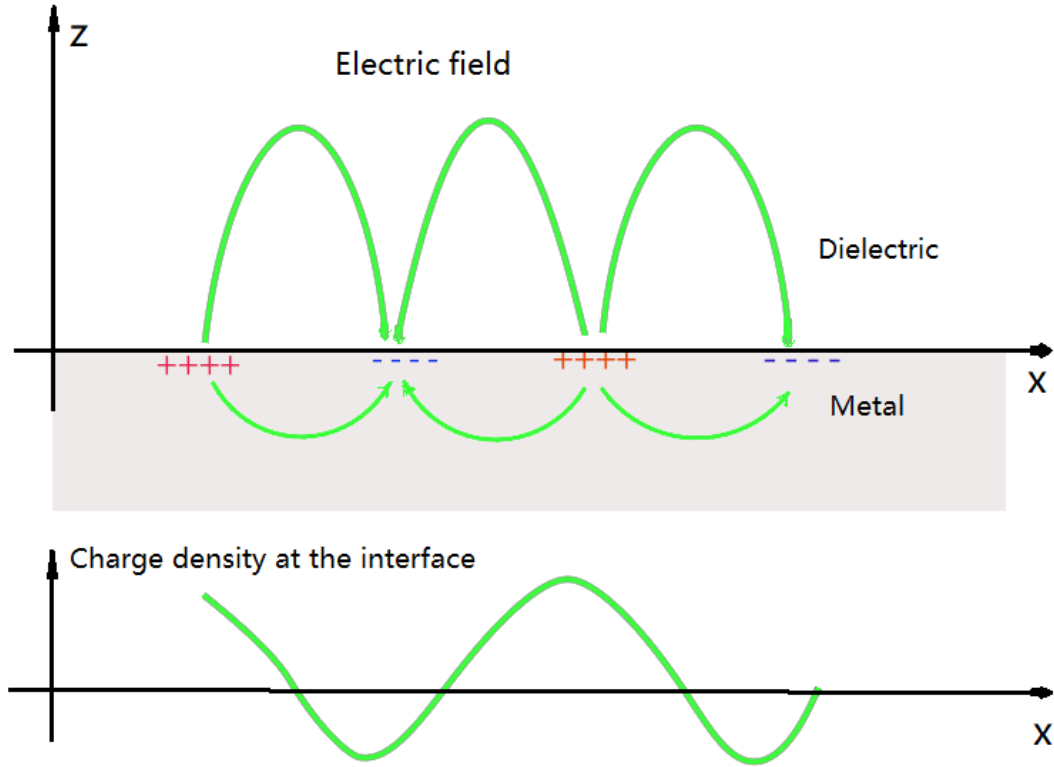


Figure 2.1: Schematic illustration of electromagnetic wave and surface charges at the interface between the metal and the dielectric material.

Using a dielectric whose dielectric function and magnetic permeability are ϵ_1 and μ_1 respectively, with the interface in the $x-y$ plane (metal (ϵ_2, μ_2)), we obtain the formula for the absolute value of the reflection coefficient of the p -polarized wave (also called transverse magnetic wave) using

$$|r_p| = \left| \frac{\epsilon_2 / \epsilon_1 - q_{z,2} / q_{z,1}}{\epsilon_2 / \epsilon_1 + q_{z,2} / q_{z,1}} \right| \quad (2.2)$$

and the corresponding one for the s -polarized wave (also called transverse electric wave)

$$|r_s| = \left| \frac{\mu_2 / \mu_1 - q_{z,2} / q_{z,1}}{\mu_2 / \mu_1 + q_{z,2} / q_{z,1}} \right| \quad (2.3)$$

in which the z -component of the wavevectors are defined q_z as

$$q_{z,1} = \sqrt{\left(\frac{\omega}{c}\right)^2 \varepsilon_1 \mu_1 - q_x^2} \quad (2.4)$$

$$q_{z,2} = \sqrt{\left(\frac{\omega}{c}\right)^2 \varepsilon_2 \mu_2 - q_x^2} \quad (2.5)$$

Notice that for p -polarized wave, it's the electric component that propagates along the interface while it is the magnetic component for s -polarized wave (which would be called magnetic plasmon polariton).

With these formulas at our disposal, we are about to embark on the dispersion relations for different occasions. Firstly, r_p diverges (namely denominator equals zero) for

$$\varepsilon_2 / \varepsilon_1 + q_{z,2} / q_{z,1} = 0 \quad (2.6)$$

Then we acquire the dispersion relation for electric surface plasmons after substituting equations (4), (5) into (6), which can be written as

$$q_x^2 = \left(\frac{\omega}{c}\right)^2 \cdot \frac{\varepsilon_1^3 \mu_1 - \varepsilon_2^3 \mu_2}{\varepsilon_1^2 - \varepsilon_2^2} \quad (2.7)$$

It can be reduced to a more familiar form for non-magnetic dielectric

$$q_x = \frac{\omega}{c} \sqrt{\frac{\varepsilon_1 \varepsilon_2}{\varepsilon_1 + \varepsilon_2}} \quad (2.8)$$

Providing the Drude model $\varepsilon(\omega) = 1 - \omega_p^2 / \omega^2$ in which $\omega_p = \sqrt{\frac{4\pi n e^2}{m}}$, and $\varepsilon_1 = 1$ when the dielectric is vacuum, the dispersion relation (one can find it in Fig. (2.2)) for SPP can be obtained as

$$q_x = \frac{\omega}{c} \sqrt{\frac{1 - \frac{\omega_p^2}{\omega^2}}{2 - \frac{\omega_p^2}{\omega^2}}} \quad (2.9)$$

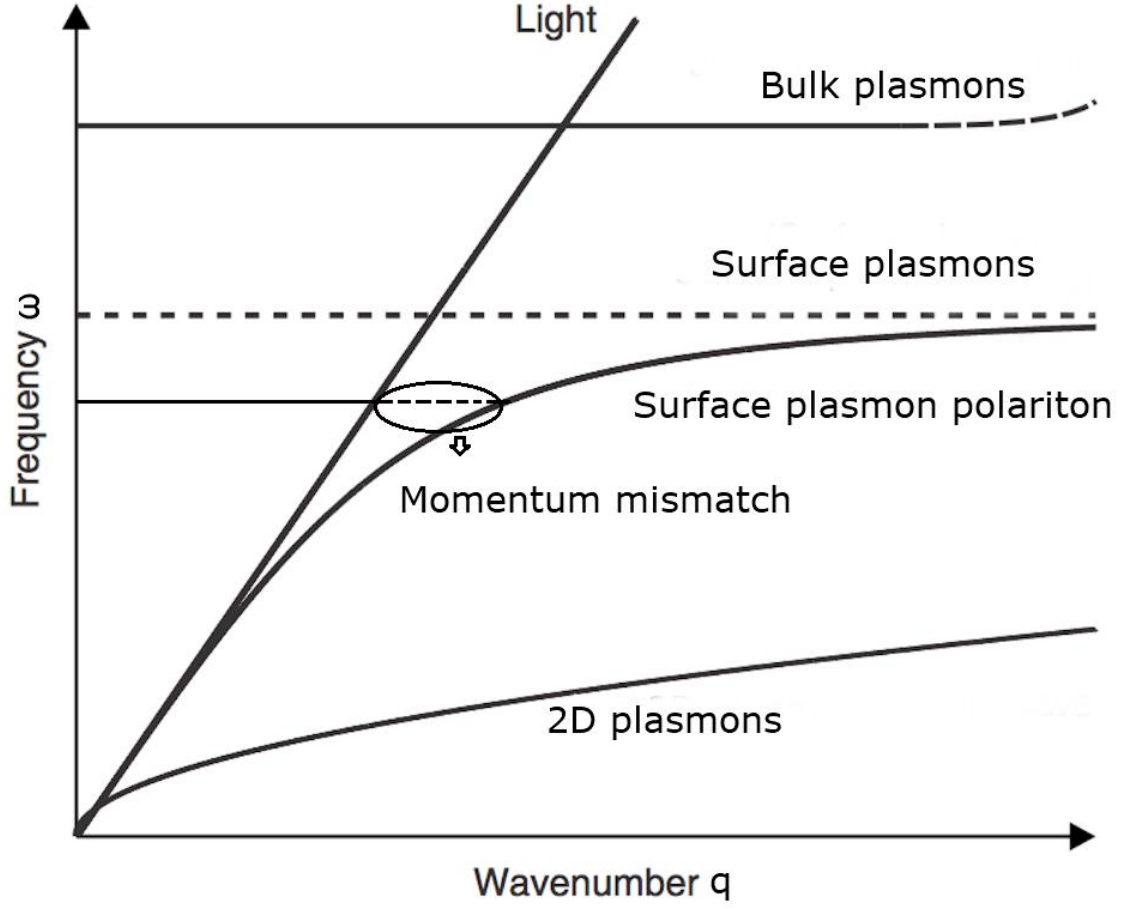


Figure 2.2: Dispersion relations for light wave, bulk plasmons, surface plasmons, surface plasmon polariton and 2D plasmons. Reprinted figure from H. Yoon [16].

Surface plasmon frequency is defined as the asymptotic limit after setting q_x in Eq. 2.9 to be infinite,

$$\omega_{sp} = \frac{\omega_p}{\sqrt{1 + \epsilon_2}} \quad (2.10)$$

From Eq. (2.10) one can conclude that when the sum of the dielectric function of the dielectric (vacuum in this case) and the metal (surrounding the interface) equals zero, surface plasmon effect would happen.

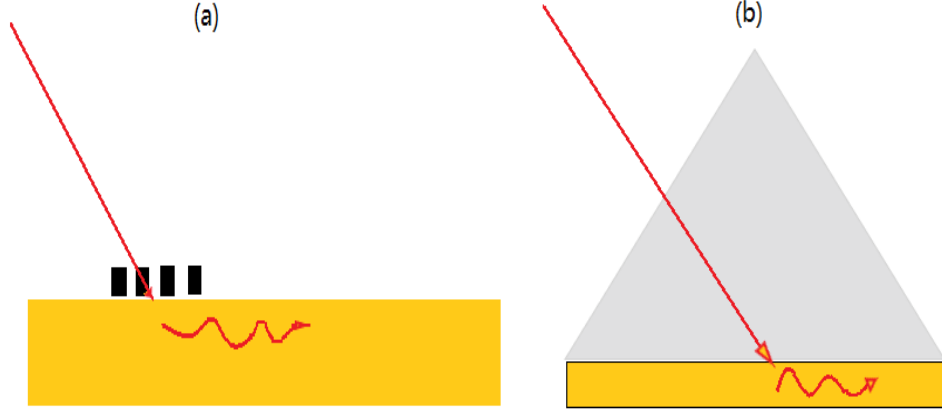


Figure 2.3: Two ways to excite plasmon. (a) Grating pattern, (b) Prism on the surface of metal (Kretschmann configuration). Here yellow material is the conductive layer, gray triangular object is the prism, and red lines denote the light beam.

The wavenumber of light is lower than that of plasmons given the same frequency, which indicates that it's impossible to excite surface plasmon wave directly using photon, thus there are two main methods adopted by experimentalists to eliminate the momentum mismatch between photon and surface plasmon wave. The first method involves introducing features onto the surface of the conductive material, such as surface roughness or a grating pattern (Fig. 2.3 (a)).

This method is based on the diffraction effects by a diffraction grating or a surface feature. When the light incident on the grating is at an angle θ from the normal direction and has wavenumber q , extra momentum can be added to the light from the grating structure, then if the following condition is met, the SPP effect can be excited.

$$\beta = |k| \sin \theta \pm \nu g, \quad (2.25)$$

in which β is corresponding SPP wavevector, $g = 2\pi / a$ where a is the lattice constant and $\nu = 1, 2, 3, \dots$.

During the process of excitation, the diffracted EM wave from the periodically corrugated metal-dielectric interface have larger wave-vectors than those of the incident EM wave, and as a result, the diffraction of light by the metal grating will be coupled to the plasmons.

The second method involves using a dielectric material of refractive index ($n > 1$) to

increase the momentum of the incoming light by increasing the wavenumber ($k_1 = n \cdot k_2$). Two configurations can be used for this momentum matching method. As shown in Fig. 2.3(b), in Kretschmann configuration [17], the in-plane component of the EM wave in the prism coincides with the SPP wave-vector on an air-metal interface, which gives rise to the light tunnelling through the metal film, and as a result, the light is coupled to the plasmons.

2.1.3 Two-dimensional material nanophotonics

Plasmons supported by 2D materials don't suffer significant propagating loss as typical plasmons do, thus is advantageous beyond typical SPP in terms of its long propagating distance and tunability [16]. Two-dimensional materials, also referred to as single layer materials or van der Waals materials [18], are ultrathin crystalline materials composed of one or a few layers of atoms, and these types of layered crystalline structures give rise to the unique properties of 2D materials making them a promising platform for building electronic devices [3], optoelectronic devices and also application in the catalysis and energy fields. The family of 2D materials are mainly categorized into five classes, which are respectively graphene and other single-element two-dimensional materials [19], hexagonal boron nitride (hBN) [20], transitional metal dichalcogenides (TMDC) [21], main-group metal chalcogenides [22] and alloy involved heterostructures [23] respectively.

The plasmon effect within two-dimensional (2D) materials has also been arousing tremendous research interest recently due to its fascinating properties in nanophotonics. V. I. Fal'ko *et.al.* [24] detailed the procedure of deducing the dispersion relation. Considering a 2D layer with conductivity σ (the property links the current density to the electric field for general frequencies) which is parallel to the plane and perpendicular to the z direction. The complete set of Maxwell Equations for the vector $\vec{A} = (A_x, A_y, A_z)$ and scalar potential φ is proposed [24]

$$\left(\frac{1}{c^2} \frac{\partial^2}{\partial t^2} - \nabla^2 \right) \begin{pmatrix} \varphi \\ \vec{A} \end{pmatrix} = \begin{pmatrix} 4\pi\rho \\ 4\pi\vec{j}/c \end{pmatrix} \delta(z) \quad (2.11)$$

$$\nabla \cdot \vec{A} + \frac{1}{c} \frac{\partial \varphi}{\partial t} = 0 \quad (2.12)$$

$$\vec{j} = -\sigma \left(\nabla \varphi + \frac{1}{c} \frac{\partial \vec{A}}{\partial t} \right) \quad (2.13)$$

Starting from the assumption that natural oscillations are propagating along the 2D layer in the form of a wave $\exp(i\vec{q} \cdot \vec{r} - i\omega t)$ and localized near the layer. The vector and scalar potentials are therefore proportional to $\exp(-\beta z)$, here $\beta = \sqrt{q^2 - \frac{\omega^2}{c^2}}$, $\text{Re}(\beta) > 0$ and $\text{Im}(\beta) < 0$ if it is a complex number. Due to the fact that charge carriers are confined within 2D layer, \vec{j} is also parallel to the 2D plane which would cause A_z to be zero. Thus the vector potential \vec{A} only has elements in the 2D layer plane, which can be further rewritten as $\vec{A} = (\vec{q}/|q|)A_{\parallel} + (\vec{q} \times I_z)A_{\perp}$.

Solving the set of Maxwell Equations for TM mode, namely $E_{\perp} = -\frac{\partial}{\partial_{\perp}}\varphi - \frac{1}{c}\frac{\partial}{\partial_{\perp}}\vec{A} = 0$ or $A_{\perp} = 0$, then

$$\begin{aligned} \nabla \cdot \vec{A} + \frac{1}{c} \frac{\partial \varphi}{\partial t} &= 0 \Rightarrow i\vec{q} \cdot \vec{A} + (-i\omega)\varphi = 0 \\ \Rightarrow \varphi &= \frac{\vec{q} \cdot \vec{A}}{\omega} \end{aligned}$$

Therefore

$$\begin{aligned} \vec{j} &= -\sigma \left(\nabla \varphi + \frac{1}{c} \frac{\partial \vec{A}}{\partial t} \right) = -\sigma \left(i\vec{q}\varphi + \frac{-i\omega}{c} \vec{A} \right) \\ &= -\sigma \left(i\vec{q} \frac{\vec{q} \cdot \vec{A}}{\omega} + \frac{-i\omega}{c} \vec{A} \right) \end{aligned}$$

And from Eq. (2.11) we can get

$$\begin{aligned} \left(\frac{1}{c^2} \frac{\partial^2}{\partial t^2} - \nabla^2 \right) \vec{A} &= \frac{4\pi\vec{j}}{c} \delta(z) \\ \Rightarrow -2\beta A(z=0) &= \frac{4\pi\vec{j}}{c} \end{aligned}$$

Then the dispersion relation is obtained as [24]

$$1 + i \frac{2\pi\sigma}{\omega} \sqrt{q^2 - \frac{\omega^2}{c^2}} = 0 \quad (2.14)$$

In the non-retarded regime ($q \gg \omega/c$), the relation can be rewritten as [24]

$$q_{TM} = \frac{i\omega}{2\pi\sigma} \quad (2.15)$$

For TE mode which is not applicable in the 3D SPP case, $E_{\parallel} = E_z = 0$, thus the dispersion relation can be written as [24]

$$\sqrt{q^2 - \frac{\omega^2}{c^2}} - i \frac{2\pi\sigma}{c} \frac{\omega}{c} = 0 \quad (2.16)$$

which in the non-retarded regime reduces to

$$q_{TE} = \frac{2i\pi\sigma\omega}{c^2} \quad (2.17)$$

With the specific example of graphene, M. Jablan *et. al.* [25] gave two approaches to calculate the dispersion relation, one is the classical approach using Drude like expression

$$\sigma(\omega) = \frac{e^2 E_F}{\pi \hbar^2} \frac{i}{\omega + i\tau^{-1}} \quad (2.18)$$

where $E_F = \hbar v_F \sqrt{\pi |n|}$, $v_F = 10^6 \text{ m/s}$ is the Fermi velocity of graphene, τ the relaxation-time, and n the charge carrier density. When damping rate τ is extremely high, one can get the dispersion relation (one can find it in Fig. (2.2)) after substituting Eq. (2.18) to Eq. (2.15)

$$\omega = \frac{e}{\hbar} \sqrt{E_F \cdot q} \quad (2.19)$$

Another is the quantum mechanical approach which directly uses the dielectric function obtained from the self-consistent field approach [26], and let the dielectric function to be zero, then one can get the similar dispersion relation $\omega \propto q^{1/2}$ as in the classical model. More details can be found in Sec. 2.2.

To better understand the proper scenarios of applying SPP and 2D plasmons, the connections and the differences between them will be discussed. The properties of SPP in metals are decided by the material properties like the surface geometry or charge carrier density. When the metal film is sufficiently thin, SPP at both interfaces can be coupled in symmetric and antisymmetric combinations. The symmetric mode, or short-range SPP has the electric field confined in the film as long as the film thickness is smaller than the skin depth. While 2D plasmon-polaritons (PP) can be seen as the extension of short-range SPP as the thickness approaches a certain limit, the difference between them is that SPP can only propagate much shorter distance than 2D plasmon polaritons do.

To show the relationship between 2D plasmon and SPP in a pedagogical way [27], the dispersion relation of 2D plasmons can be derived in a similar way to SPP. In our case the 2D material is embedded between medium 1 and medium 2, therefore the electromagnetic fields of TM surface wave are given as follows

$$\begin{aligned} E_x^{(1)} &= E_1 e^{iqx} e^{-\kappa_1 z} \\ E_z^{(1)} &= \frac{iq}{\kappa_1} E_z^{(1)} \\ H_y^{(1)} &= -\frac{i\omega\epsilon_1}{2\pi\kappa_1} E_x^{(1)} \end{aligned} \quad (2.20)$$

This is the relation for the fields in medium 1.

$$\begin{aligned} E_x^{(2)} &= E_2 e^{iqx} e^{\kappa_2 z} \\ E_z^{(2)} &= -\frac{iq}{\kappa_1} E_z^{(2)} \\ H_y^{(2)} &= \frac{i\omega\epsilon_2}{2\pi\kappa_2} E_x^{(2)} \end{aligned} \quad (2.21)$$

This is the relation for the fields in medium 2, where $\kappa_i = \sqrt{q^2 - \epsilon_i \omega^2 / c^2}$.

And the boundary condition is

$$\begin{aligned} E_x^{(1)} &= E_x^{(2)} \\ H_y^{(1)} - H_y^{(2)} &= -J = -\sigma(\omega) E_x^{(2)} \end{aligned} \quad (2.22)$$

Then dispersion relation can be written as

$$\frac{\varepsilon_1}{\kappa_1} + \frac{\varepsilon_2}{\kappa_2} + \frac{2\pi i \sigma(\omega)}{\omega} = 0 \quad (2.23)$$

In the nonretarded regime ($q \gg \omega / c$), it can be further simplified to

$$q \approx \frac{\varepsilon_1 + \varepsilon_2}{2\pi} \frac{i\omega}{\sigma(\omega, q)} \quad (2.24)$$

The dispersion relations of SPP and 2D plasmons are depicted in Fig. (2.2). The SPP dispersion has two asymptotes [16] at low frequencies and at frequencies approaching the surface plasmon frequency as one can get from Eq. (2.9). And one can find the frequency is proportional to the square root of wavenumber in the 2D plasmonic dispersion relation in the Eq. (2.19). At low frequencies, the metal nearly does not influence the surface wave, which propagate mostly in the dielectric. As the frequency rises, the interaction between the electromagnetic wave and the 3D bulk plasmonic oscillation dominates, causing another asymptote when wavenumbers approach infinite.

From Eq. (2.19) one can find the dispersion relation of 2D plasmonic waves deviates from the light dispersion at all frequencies, and does not show an asymptotic behavior to a particular frequency. So from the dispersion of these two kinds of plasmons, one can find that it's harder to excite 2D plasmons within the visible spectrum due to the larger momentum mismatch with light. And in the experiment scientists normally use the terahertz or far-infrared laser source to induce the plasmon effect within 2D materials [28].

2.2 Theoretical models of plasmons in quasi-two-dimensional systems

Following the previous contents, the properties of plasmons underlie the significance of dielectric function of plasmonic materials. In this section the well-established theoretical framework to get the dielectric function in three dimensions will be introduced, and it can be applied to any homogeneous multi-dimensional system. And on the base of the framework the way to get the dielectric function in quasi-two-dimensional (Q2D) system is also discussed in detail, for the sake of the application on a hydrogen terminated diamond surface as our targeted sample.

2.2.1 Self-consistent approach to obtain dielectric function

H. Ehrenreich *et al.* [29] did pioneering work in deriving the dielectric function in the system with energy split in the z direction with the self-consistent field method. The essence of the self-consistent treatment is that external perturbation redistributes the charge within the system. Afterwards the redistributed charge creates an induced potential which acts to screen the original external potential. The total self-consistent potential is composed of the original external potential Φ_{ext} plus the induced screening potential Φ_{ind} . The result of the distribution of the charge must be consistent with the total potential.

First he started with Liouville equation of motion for the density operator,

$$i\hbar \frac{\partial \rho_{op}}{\partial t} = [H, \rho_{op}] \quad (2.27)$$

and the single-particle Hamiltonian is

$$H = H_0 + V(\vec{r}, t) \quad (2.28)$$

where $H_0 = -\frac{\hbar^2}{2m} \nabla^2$ is the Hamiltonian for single free electron satisfying Schrodinger equation $H_0 \vec{k} = \varepsilon_k \vec{k}$. The eigen states for the free electron system are

$$k = \Omega^{-\frac{1}{2}} \exp(i \vec{k} \cdot \vec{r}) \quad (2.29)$$

Now the density operator is rewritten as $\rho_{op} = \rho_{op}^0 + \rho_{op}^1$ Where ρ_{op}^0 means the density operator for the unperturbed system, and ρ_{op}^1 the perturbed term.

Fourier expanding the total perturbing potential energy

$$V(\vec{r}, t) = \sum_{\vec{q}} V(\vec{r}, \vec{q}, t) \exp(i \vec{q} \cdot \vec{r}) \quad (2.30)$$

Then Eq. (2.27) becomes

$$i\hbar \frac{\partial}{\partial t} (\rho_{op}^0 + \rho_{op}^1) = \left[H_0 + \sum_{\vec{q}'} V(\vec{q}', t) \exp(i\vec{q}' \cdot \vec{r}), \rho_{op}^0 + \rho_{op}^1 \right] \quad (2.31)$$

After taking matrix between states $|\vec{k}\rangle$ and $|\vec{k} + \vec{q}\rangle$, and only considering the first-order perturbation, we therefore obtain

$$i\hbar \frac{\partial}{\partial t} \langle \vec{k} + \vec{q} | \rho_{op}^1 | \vec{k} \rangle = (\varepsilon_{\vec{k} + \vec{q}} - \varepsilon_{\vec{k}}) \langle \vec{k} + \vec{q} | \rho_{op}^1 | \vec{k} \rangle + \left[f(\varepsilon_{\vec{k}}) - f(\varepsilon_{\vec{k} + \vec{q}}) \right] V(\vec{q}, t) \quad (2.32)$$

Here $f(\varepsilon_{\vec{k}})$ is the distribution function for charge carriers, in particular the Fermi-Dirac distribution function for electrons.

Assuming that the external perturbation is proportional to $e^{-i\omega t + \eta t}$ in which η is the adiabatic item which can be set to be infinitely small after our derivation, thus the induced potential, the total potential, and the density fluctuations all have the similar dependence $e^{-i\omega t + \eta t}$ as the external potential is exerted on the system. Thus Eq. (2.32) yields

$$\langle \vec{k} + \vec{q} | \rho_{op}^1 | \vec{k} \rangle = \frac{f(\varepsilon_{\vec{k} + \vec{q}}) - f(\varepsilon_{\vec{k}})}{(\varepsilon_{\vec{k} + \vec{q}} - \varepsilon_{\vec{k}}) - \hbar\omega - i\eta t} V(\vec{q}, t) \quad (2.33)$$

Now we are seeking to find the connection between $V_{ind}(\vec{q}, t)$ and the term $\langle \vec{k} + \vec{q} | \rho_{op}^1 | \vec{k} \rangle$. The induced screening potential energy $V_{ind}(\vec{q}, t)$ is related to the induced electron density δn by Poisson's equation:

$$\nabla^2 V_{ind}(\vec{q}, t) = -4\pi e^2 \delta n \quad (2.34)$$

The charge density equals the trace of the density operator operating on the electron position operator,

$$\delta n = \Omega^{-1} \sum_{\vec{k}, \vec{q}} \langle \vec{k} + \vec{q} | \rho_{op}^1 | \vec{k} \rangle \exp(i\vec{q} \cdot \vec{r}) \quad (2.35)$$

Combining Eq. (2.34) and Eq. (2.35), we get

$$V_{ind}(\vec{q}, t) = \frac{4\pi e^2}{q^2 \Omega} \sum_{\vec{k}} \langle \vec{k} + \vec{q} | \rho_{op}^1 | \vec{k} \rangle \quad (2.36)$$

From Eq. (2.32) and Eq. (2.36), the dielectric function is obtained as

$$\varepsilon(\vec{q}, \omega) = 1 - \lim_{\eta \rightarrow 0} \frac{4\pi e^2}{q^2 \Omega} \sum_{\vec{k}} \frac{f(\varepsilon_{\vec{k}+\vec{q}}) - f(\varepsilon_{\vec{k}})}{(\varepsilon_{\vec{k}+\vec{q}} - \varepsilon_{\vec{k}}) - \hbar\omega - i\eta} \quad (2.37)$$

When the dielectric function equals zero in the solid, the solid does not react with the electric field as one can see from Maxwell Equations. Then the free electrons inside start to oscillate the same way as a sound wave. Their force is in the same direction with their amplitude. They move backwards and forwards as the amplitude aligns in that direction. In another word, there is a non-vanishing response even to vanishing external fields, thus forming a collective oscillation. So we can get the dispersion relation after setting the dielectric function to be 0.

When this approach is applied to a 2D case, for the long-wavelength limit ($k_F \gg q \gg \omega/c$) the plasmon dispersion relation can be obtained after setting the dielectric function to be 0

$$\omega_L^2 = \frac{N_s e^2 q}{2\bar{\varepsilon}(\omega, q) \varepsilon_0 m_p} \quad (2.38)$$

Here N_s is the surface charge density, q the plasmon wave vector, $\bar{\varepsilon}(\omega, q)$ the effective permittivity, and m_p the plasmon mass.

For the detailed derivation process, readers are referred to Chapter 7 in [30].

2.2.2 Calculation of the dielectric function within quasi-2D system

When the charge carriers are confined within a thin layer, there would be a quantum energy level split in the confining direction, i.e. z axis in our context. It is called a quasi-two-dimensional system. J. Lee *et al.* [31] first proposed the application of a

self-consistent approach in the quasi-2D case. In J. Lee *et al.*'s case they used the infinite square well as the confining potential, and N. Q. Khanh [32] followed their example but utilized explicit expression for dielectric function [33] rather than the Thomas-Fermi approximation in J. Lee *et al.*'s work [31], and K. H. Aharonyan [34] extended the work to the finite square well, proving that whether in infinite or finite square well the dispersion relation in large q regime exhibit a different curve instead of relation $\omega \propto \sqrt{q}$.

To start with the derivation the energy eigenvalues for the Q2D system can be written as

$$E_{k,n} = \frac{\hbar^2 k^2}{2m_{\parallel}^* \cdot m_e} + E_n \quad (2.39)$$

Here $k=(k_x, k_y)$ is the 2D wave vector of the charge carrier, m_{\parallel}^* the relative in-plane effective mass which is non-unit, m_e the mass of electron, and n the subband number for z direction. Therefore the wave function for the hole system can be treated as

$$\Psi_k(r_{\parallel}, z) = \frac{1}{\sqrt{A}} e^{ikr_{\parallel}} \cdot \zeta_l(z) \quad (2.40)$$

in which ζ_l is the wavefunction of quantized state in z direction with quantum number to be l , and A the area of the $x-y$ plane.

The induced electron density can be obtained utilizing the Ehrenreich-Cohen self-consistent field prescription [29]

$$\rho'(r_{\parallel}, z) = 2 \sum_{k, \text{band}} \rho'_{k, \text{band}} \Psi_k^*(r_{\parallel}, z) \Psi_{k'}(r_{\parallel}, z) \quad (2.41)$$

here the density fluctuation

$$\rho'_{k, \text{band}} = \frac{f_0(E_{k'}) - f_0(E_k)}{E_{k'} - E_k + \hbar\omega - i\hbar\delta} \langle k' | V(r_{\parallel}, z) | k \rangle \quad (2.42)$$

the ket $|k\rangle$ means the whole wavefunction $\Psi_k(r_{\parallel}, z)$.

The induced charge density $n'(r_{\parallel}, z)$ can be related to the induced potential V^s via Poisson equation

$$\Delta V^s = -\frac{e^2}{\varepsilon_r \varepsilon_0} \rho'(r_{\parallel}, z) \quad (2.43)$$

By taking the 2D Fourier transform

$$V_q^s(z) = \frac{1}{\Omega} \int dr_{\parallel} V^s(r_{\parallel}, z) \exp(-iqr_{\parallel}) \quad (2.44)$$

we obtain

$$\frac{d^2 V_q^s(z)}{dz^2} - q^2 V_q^s(z) = \begin{cases} -\frac{2e^2}{\varepsilon_r \cdot \varepsilon_0 \cdot A} \sum_{k, \text{band}} \rho_{k, \text{band}}' \zeta_1(z)^2 \cdot \delta_{k-k'+q}, & x < 0 \\ 0, & x \geq 0 \end{cases} \quad (2.45)$$

Since the conducting medium is bordered by vacuum to the upside, the boundary conditions which the potential V^s has to satisfy are

$$V_q^s(0^+) = V_q^s(0^-), \frac{dV_q^s(0^+)}{dz} = \varepsilon_r \frac{dV_q^s(0^-)}{dz} \quad (2.46)$$

The relation between induced potentials and total potentials is as follows

$$\langle l' | V_q^s(z) | l \rangle = \sum_{k, \text{band}} 8\pi \chi_{k'kl'l} \langle k' | V_q^s(r_{\parallel}, z) | k \rangle \delta_{k'-k+q}, \quad (2.47)$$

here $|l\rangle$ stands for the wave function in z direction with subband number l .

And the polarization terms are given by

$$\chi_{k'kl'l} = \frac{e^2}{\varepsilon A} \frac{f_0(E_{k'}) - f_0(E_k)}{E_{k'} - E_k + \hbar\omega - i\hbar\delta} R_{k'kl'l} \quad (2.48)$$

$$R_{k'kl'l} = \int dz V_q^s(z) \zeta_{l'}(z) \zeta_l(z) \quad (2.49)$$

Then we can get the dielectric function as

$$\varepsilon_{n',n,l',l} = \left(\delta_{nl} \delta_{n'l'} - \sum_k 8\pi \chi_{\vec{k}+\vec{q},n';\vec{k},n;n'l'} \right) \quad (2.50)$$

Then it's straightforward to get the dispersion relation from the dielectric function after setting it to be zero. Here we revisit the self-consistent approach to obtain dielectric function for Q2D systems, which takes into consideration the energy split which stems from the z

direction confinement. For inversion layer in semiconductors, which would involve the triangular potential well in the z direction, the improved precision will help us get better evaluation of the screening effect and the scattering rate.

2.3 Optical explorations for plasmonic dielectric functions on two-dimensional materials

After reviewing the fundamental theories of plasmonics, we are now seeking to experimentally realize the plasmonic excitations. Ellipsometry is the common experimental method to obtain the dielectric functions, which would help us verify the theoretical results. And scanning near-field optical microscopy (SNOM) combines optical microscopy and atomic force microscopy, which offers us a versatile platform to probe plasmonic excitation.

2.3.1 Ellipsometry measurement

Other than the theoretical derivation of dielectric function, we are also seeking to measure it directly by the means of ellipsometry, thus we will be able to verify the theoretical results.

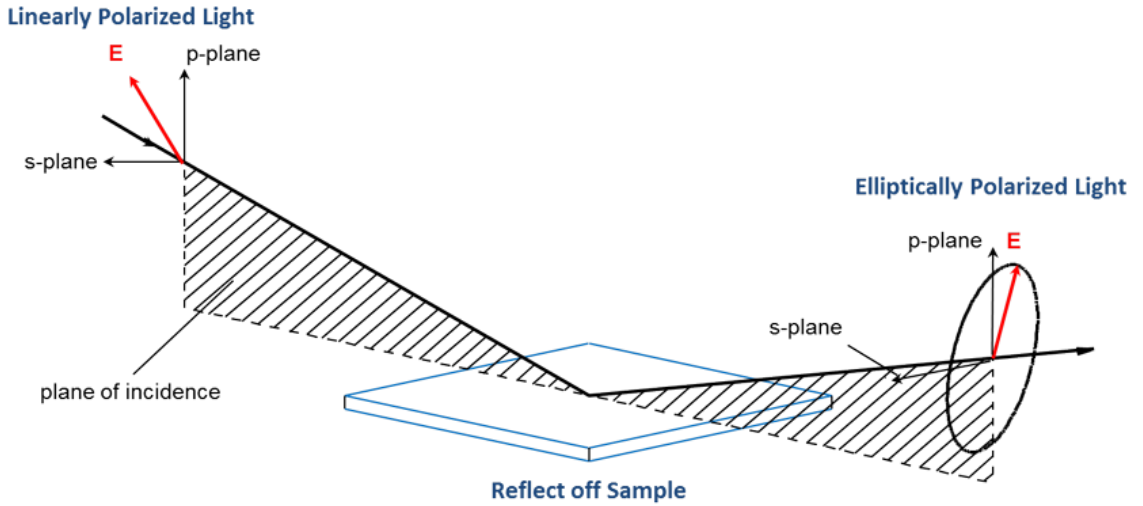


Figure 2.4: Schematic setup of an ellipsometry experiment. Reprinted from JA Woollam Ellipsometry manual [35].

Consider the reflection of polarized light from a sample when light is obliquely reflected

from a sample. The incident and reflected beams define a plane of incidence, and the incidence light with its electric field vector oscillating in the plane of incidence is called p polarized light, while light with its electric field vector oscillating perpendicular to the plane is called s polarized light. The enabling principle of ellipsometry is that p and s polarized light reflects differently. The angle of incidence is chosen close to the Brewster angle of the sample to ensure a maximal difference. Ellipsometry measures the complex reflectivity ratio of p and s polarized light and typically reports the results in terms of the amplitude ratio Ψ upon reflection, and Δ is the phase shift.

$$\rho = \frac{r_p}{r_s} = \tan(\Psi) e^{i\Delta} \quad (2.51)$$

With the experimental results at our disposal, we still need to find a proper model to inverse the dielectric function from these data. The simplest model is to deal with a single interface between two homogeneous and isotropic media with infinite thickness, 0 and 1, the reflection coefficients are given by the Fresnel formulas [1]

$$r_{01p} = (\varepsilon_1 S_0 - \varepsilon_0 S_1) / (\varepsilon_1 S_0 + \varepsilon_0 S_1) \quad (2.52)$$

$$r_{01s} = (S_0 - S_1) / (S_0 + S_1) \quad (2.53)$$

in which ε_i is the dielectric function of the i th medium, and $S_i = (\varepsilon_i - \varepsilon_0 \sin^2 \theta)^{1/2}$ with θ being the angle of incidence in medium 0.

Then dielectric function is given by

$$\varepsilon_1 = \varepsilon_0 \left\{ \sin^2 \theta + \sin^2 \theta \tan^2 \theta \left[(1 - \rho) / (1 + \rho) \right]^2 \right\} \quad (2.54)$$

For light incident from a medium of known ε_0 , Eq. (2.54) determines the complex dielectric function ε_1 of the reflecting second medium in terms of the measured ρ and the angle of incidence θ .

2.3.2 Scanning near-field optical microscopy

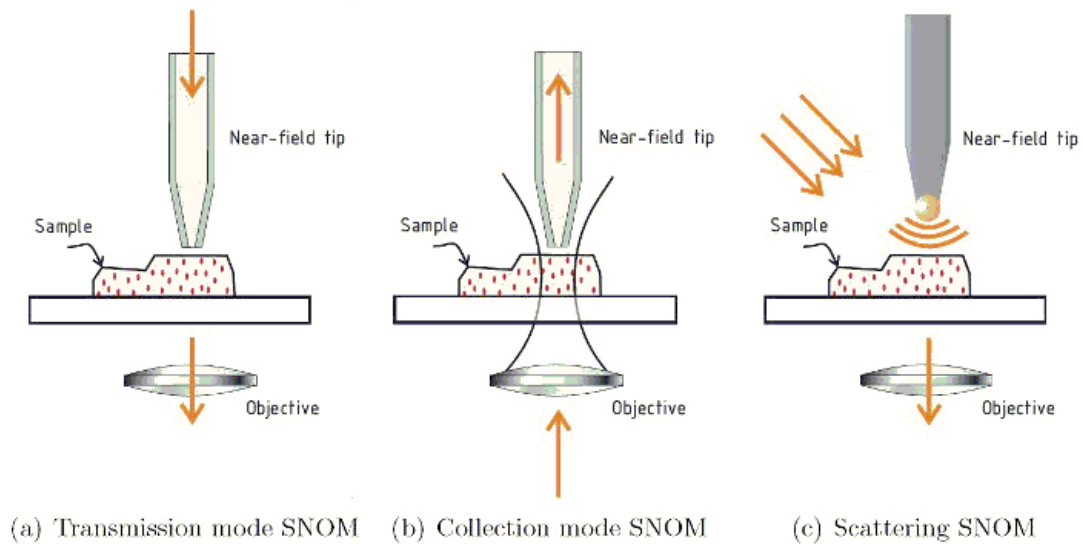


Figure 2.5: Different types of scanning near-field optical microscopes [2]: (a) Transmission mode for aperture SNOM, (b) collection mode for aperture SNOM, (c) apertureless SNOM.

Due to the restriction of the Rayleigh diffraction limit, optical microscopes can hardly achieve resolutions above half the wavelength of the light source used [1]. Thus scientists resort to the methods which reduces the wavelength of the beam source, like the scanning electron microscopy (SEM) [36] and the transmission electron microscopy (TEM) [37], or they take advantage of the quantum tunneling of electrons between the surface and the tip, like scanning tunneling microscopy (STM) [38]. These new types of microscope have brought fabulous gains in resolution up to the atomic level.

However these gains in resolution come at the expense of the spectroscopic capabilities, high temporal resolution, and polarization properties which are more accessible and informative in most applications. Furthermore, most of these high resolution techniques require conductivity and vacuum compatibility, which are hardly applicable for most biological specimens. The emergence of scanning near-field optical microscopy (SNOM) makes it possible to take advantage of the spectroscopic properties to achieve superior resolutions.

In SNOM, the laser beam is focused through an aperture with a diameter smaller than the excitation wavelength, resulting in a near field on the far side of the aperture. When the sample is mapped at a small distance below the aperture, the optical resolution is limited only by the diameter of the aperture. Nowadays the lateral resolution of 20 nm and vertical resolution of 200 nm have been demonstrated with the aperture diameter being 500 nm [2].

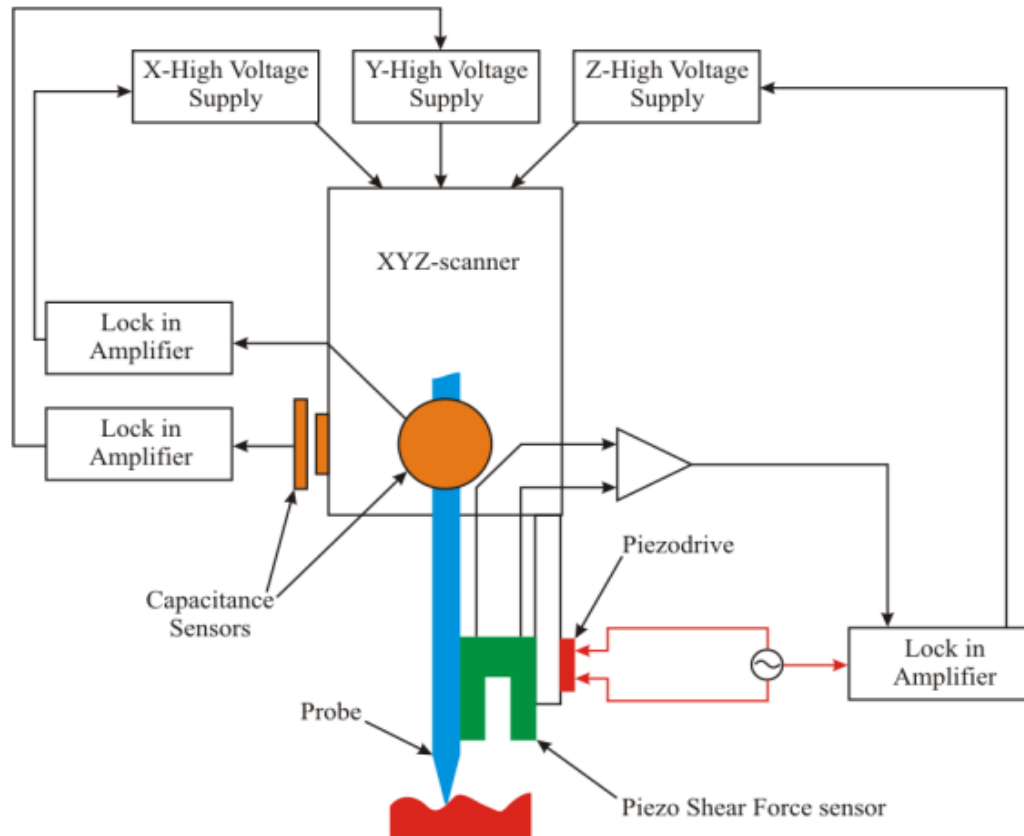


Figure 2.6: Functional schematics of the SNOM measuring head. Reprinted from NTEGRA Solaris Probe NanoLaborator Instruction Manual [39].

Currently, two types of SNOM are in use [2]: aperture SNOM and scattering SNOM (also called apertureless SNOM). Aperture SNOM uses a sub-wavelength aperture for the light confinement. The resolution typically reaches a value of about 50 to 100 nm . While Scattering SNOM is based upon the interaction of the optical near-field of a sharp metal or the dielectric tip with the sample. Basically, a laser spot is focused (limited by diffraction) onto the tip and excites it to coupled optical/electronic oscillations. The corresponding field

concentration at the tip apex is similar to the lightning rod effect in electrostatics.

As one can tell from Fig. (2.5 c), a relatively larger area of the sample around the tip is exposed to the laser light, resulting in low signal-noise ratio. Our lab works with the aperture SNOM produced by NTEGRA Solaris Probe NanoLaboratory to work on 2D materials and biological samples.

As depicted in Fig. (2.6), a tuning fork is mounted alongside the tip and made to oscillate at its resonance frequency. The amplitude is closely related to the tip-surface distance, and thus used as a feedback mechanism. Movements of the scanner in the XY plane are controlled by means of the capacitance sensors. A piezo vibrator is located at the place where the probe is fixed to the scanner. It oscillates at the resonance frequency of the system consisting of the probe, quartz resonator and probe holder. The signal is read from the contacts of the quartz resonator. It is proportional to the oscillation amplitude of the resonator. During the approach of the probe to the sample surface, the resonance frequency of the system changes due to the influence of the atomic interactions between the probe tip and the surface.

Graphene is a typical 2D material which is easy to fabricate and superior in optoelectric properties for the realization of plasmonic excitation. Two groups [40,41] nearly simultaneously managed to probe propagating plasmon polariton within graphene in 2012. In this experimental method (Fig. (2.7)), an IR beam is used to shine on a metallic AFM tip, which allows the tip to “emit” radiation over a large range of momentum space that can be used to locally launch SPP in graphene. If the wavelength of the incident light is kept at a constant level ($\lambda_0 = 9.7 \mu m$), the formed SPP can propagate along with the rationally defined graphene structures. The edge-reflected SPP waves interfere with incoming SPP waves and form localised standing waves which can be probed by collecting the emitting light, which is decoupled from the polariton in the near field from the surface.

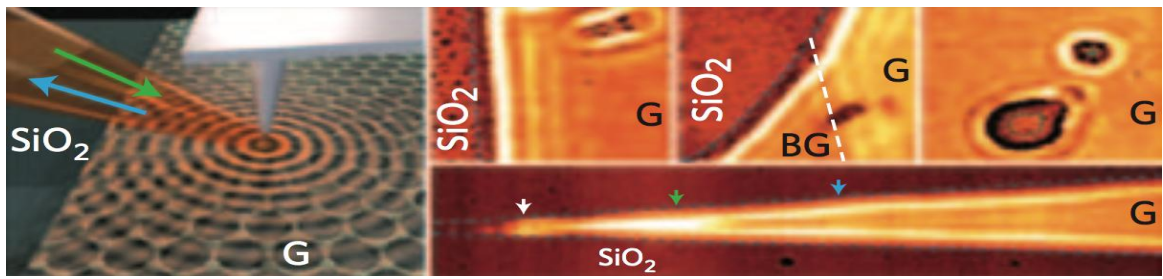


Figure 2.7: Schematic of SNOM measurement for probing plasmon on graphene, where the probe tip is excited with a laser source, launching plasmons radially from the tip, with the scattered plasmons also collected by the tip Reprinted figure from Z. Fei *et al.* [41].

Dielectric function and plasmon dispersion relation of a quasi-two-dimensional hole gas on hydrogen terminated diamond surface

3.1 Introduction

The development of plasmonics has led to remarkable fundamental insights into the interaction between light and matter at the nanoscale [42], allowing the diffraction limit to be circumvented and novel imaging/sensing techniques to be created. This enables the development of nano-optics, which takes the advantage of nanostructured materials possessing extraordinary optical properties not found in their macroscopic counterparts. The recent realization of plasmonic excitation in different 2D van der Waals materials [43] gives researchers new impetus to look for new plasmonic effects in 2D or Quasi-2D (Q2D) electron systems. Van der Waals type 2D materials, which are intrinsically 2D in nature, are usually synthesised through chemical vapor deposition (CVD), molecular beam epitaxy (MBE) or isolated from bulk crystals by mechanical exfoliation. In contrast, Q2D electron systems are commonly realized through quantum-wells, heterojunction or superlattices with semiconducting components [44].

The dielectric function is an important property to infer plasmonic properties; for this reason, significant research efforts have been devoted to theoretical studies of the dielectric function of 2D and/or Q2D electronic systems. Stern [26] did the pioneering work in deriving the dielectric function with the polarizability given by self-consistent-field treatment. Afterwards Alexander Fetter and V. A. Volkov et. al. obtained the exact analytic form of the dielectric function by using the hydrodynamic method [45,46] and Maxwell's equation with boundary conditions [47]. Ehrenreich et. al. [29] first applied the self-consistent field approach to get the dielectric function when there is energy split in the z direction, which then is extended by Lee et. al. and Backes et. al. on Q2D materials to include intra and inter-subband interaction separately [31], and simultaneously [48]. Nguyen [32] revisited

the result of Lee when confinement in the z direction is characterized by an infinite potential well and obtained the dispersion relation of plasmons. Recently, the finite potential well [34], δ -potential [49], triangular potential [50], and time dependent self-consistently screened triangular potential [51] were also investigated, highlighting the considerable difference in properties between Q2D and pure 2D systems.

An experimental realization of a Q2D charge carrier system is the surface transfer doping of hydrogen terminated diamond [4], which allows the diamond surface to support a p-type surface conductivity with an underlying sub-surface Q2D hole accumulation confined by an upward band bending [52]. The robustness of the hole gas in diamond and the transparency of diamond over a wide range of the electromagnetic spectrum makes it a promising opto-electronic material for bio-sensing applications.

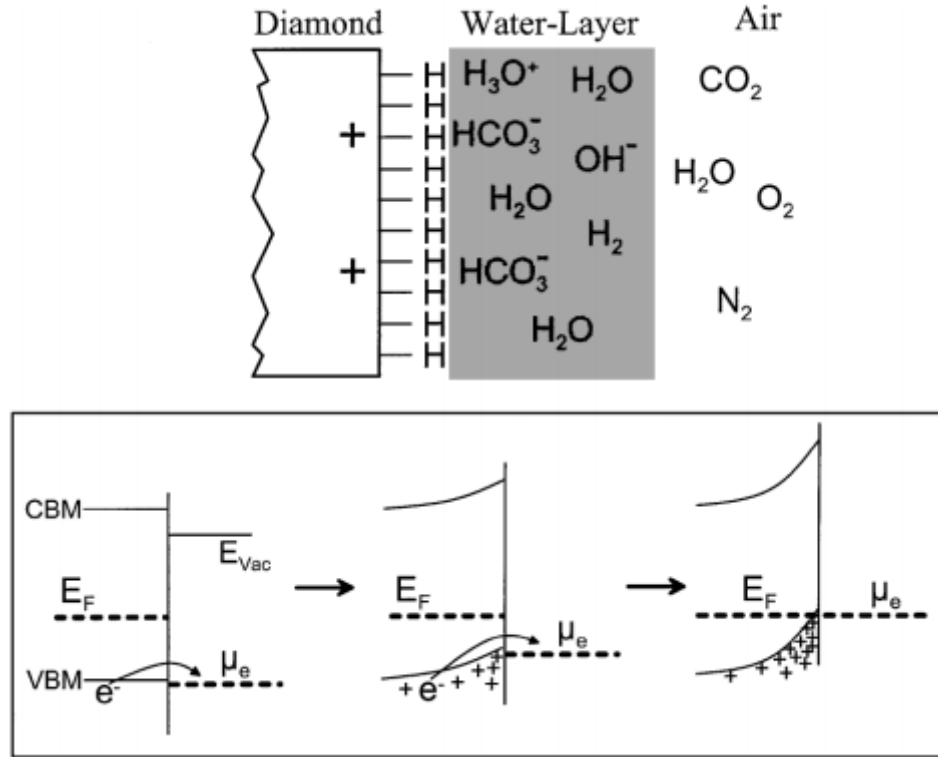


Figure 3.1: Schematic picture of the hydrogenated diamond surface doped by water. Bottom: Evolution of band bending at the diamond-water interface. Reprinted from [52].

Meanwhile there has been no established approach to evaluate the plasmon properties of the 2D hole gas on hydrogen terminated diamond, so the main purpose of this chapter is to determine the dielectric function for a Q2D hole gas confined in a triangular potential well,

following the method developed by Lee et al. [31]. The plasmon dispersion relationship in the Q2D system will be analyzed with the confining potential being a triangular one, which has not been presented before, providing significant insights into the future development of potential hole plasmonic devices. We first derive a numerical method to calculate the induced potential in the 2D Fourier space, and then obtain the dispersion relation for different effective electric field strengths. It will be shown that when the effective electric field strength becomes large, the dielectric function of the Q2D system reduces to that of the 2D system. We also calculate the static dielectric function to assess the screening effect in both the 2D and Q2D cases.

3.2 Model of a confined hole gas

The wave function of a hole in a 2DHG can be written as the product of the in-plane (x,y) free hole gas wave function and the wave function perpendicular to the 2D surface

$$\Psi_{kl}(r_{\parallel}, z) = \frac{1}{\sqrt{A}} e^{ikr_{\parallel}} \cdot \zeta_l(z) \quad (3.1)$$

where k is the wave number of in-plane (x, y) , $r_{\parallel} = (x, y)$, and A is the area of the hydrogenated surface. The holes are confined by a potential well arising from charge separation between accumulated holes on diamond and electrons on surface acceptors [53], thus the carriers are put in the linear electric field, and can be approximately characterized by a triangular well, according to the observation of quantized energy level in the vertical direction [54]. In the z direction, the wave function obeys the following Schrodinger equation,

$$-\frac{\hbar^2}{2m_{\perp}^* \cdot m_e} \frac{d^2}{dz^2} \zeta_l(z) - eFz \zeta_l(z) = E_l \zeta_l(z) \quad (3.2)$$

where m_e is the electron mass, and $F = \frac{1}{\epsilon \cdot \epsilon_0} n \cdot e$ is the electric field strength. Using typical values for diamond ($\epsilon = 5.5$, density $n = 10^{13} \text{ cm}^{-2}$ and relative effective mass in the z direction $m_{\perp}^* = 0.5365$ [4]) yields $F = 3.287 \times 10^{8} \text{ V/m}$.

Therefore one can write the solution to the Schrodinger equation as

$$\zeta(z) = C \cdot Ai \left[\left(\frac{2m_{\perp}^* \cdot m_e}{-\hbar^2 e^2 F^2} \right)^{\frac{1}{3}} (-eFz - E_l) \right] \quad (3.3)$$

where Ai is the Airy function, and C is a proportionality constant which can be determined by normalization. The eigenvalues E_l are obtained from

$$E_l = - \left(\frac{\hbar^2}{2m_{\perp}^* \cdot m_e} \right)^{\frac{1}{3}} \cdot \left(\frac{3\pi eF}{2} \left(l - \frac{1}{4} \right) \right)^{\frac{2}{3}} \quad (3.4)$$

The Fermi energy is far below the ground state dispersion curve of the light hole band, and the conducting surface layer is so thin ($\approx 5nm$) [4] that the energy differences between different subbands are very large as in the Fig. (3.2). Thus only the ground state of heavy holes is considered.

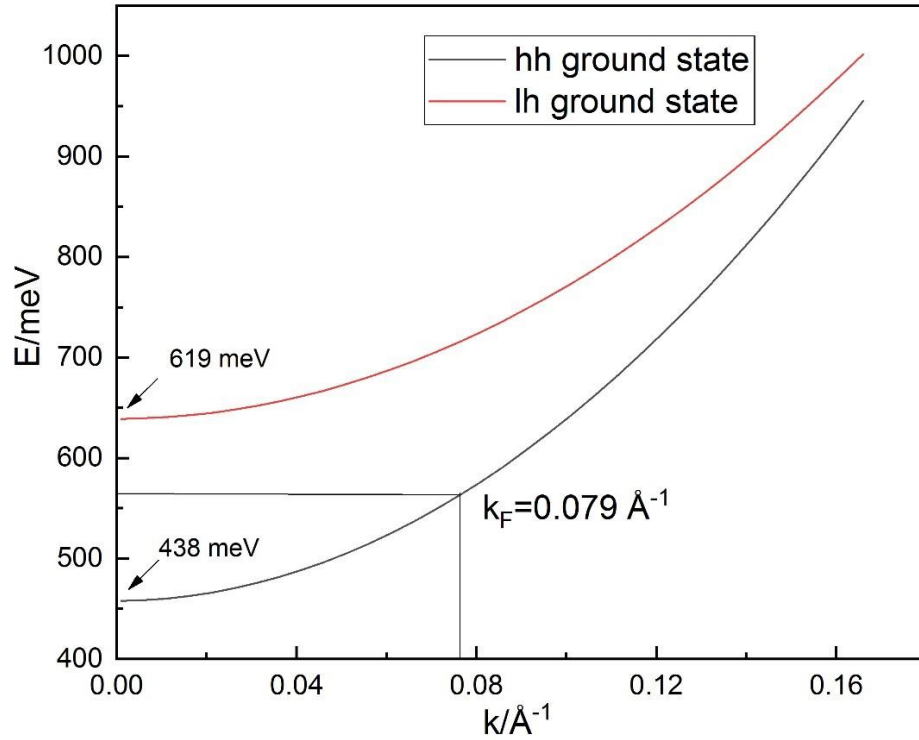


Figure 3.2: Two dimensional hole dispersion relation in a triangular well for carriers whose density is 10^{13} cm^{-2} .

3.3 Calculation of dielectric function of Q2D hole gas

The energy eigenvalues for the system can be written as

$$E_{kl} = \frac{\hbar^2 k^2}{2m_{\parallel}^* \cdot m_e} + E_l \quad (3.5)$$

Here m_{\parallel}^* is the in-plane effective mass.

The induced electron density can be obtained utilizing the Ehrenreich-Cohen self-consistent field prescription [29]

$$\rho'(r_{\parallel}, z) = 2 \sum_{kl, \zeta} \rho'_{kl, \zeta} \Psi_{kl}^*(r_{\parallel}, z) \Psi_{k'l'}(r_{\parallel}, z) \quad (3.6)$$

in which the factor 2 arises from spin degeneracy, and the density fluctuation is given by

$$\rho'_{kl, \zeta} = \frac{f_0(E_{k'l'}) - f_0(E_{kl})}{E_{k'l'} - E_{kl} + \hbar\omega - i\hbar\delta} \langle k'l' | V(r_{\parallel}, z) | kl \rangle \quad (3.7)$$

where the ket $|kl\rangle$ means the whole wavefunction $\Psi_{kl}(r_{\parallel}, z)$.

Moreover, to find the ratio between the induced and total potential, the induced charge density $n'(r_{\parallel}, z)$ can be related to the induced potential V^s via the Poisson equation

$$\nabla^2 V^s = -\frac{e^2}{\epsilon\epsilon_0} n'(r_{\parallel}, z) \quad (3.8)$$

By taking the 2D Fourier transform of Eq.(3.8) using the following relationship

$$V_q^s(z) = \frac{1}{A} \int dr_{\parallel} V^s(r_{\parallel}, z) \exp(-iqr_{\parallel}) \quad (3.9)$$

we obtain

$$\begin{aligned} \frac{d^2 V_q^s(z)}{dz^2} + q^2 V_q^s(z) &= \begin{cases} -\frac{2e^2}{\epsilon \cdot \epsilon_0 \cdot A} \sum_{kl, \zeta} \rho'_{kl, \zeta} \zeta_1(z)^2 \cdot \delta_{k', k+q}, z < 0 \\ 0, z \geq 0 \end{cases} \end{aligned} \quad (3.10)$$

Since the conducting medium is sandwiched by vacuum and bulk diamond, the potential V^s has to satisfy the boundary conditions

$$V_q^s(0^+) = V_q^s(0^-), \frac{dV_q^s(0^+)}{dz} = \varepsilon \frac{dV_q^s(0^-)}{dz} \quad (3.11)$$

Notice here we only consider the 2DHG-vacuum interface; the bottom interface between the 2DHG and the bulk diamond substrate is neglected, as the hole gas is normally embedded in the diamond substrate, and the wavefunction of the hole gas decays quickly at around 5 nm below the top of the hole gas layer, we called it the effective thickness d_{eff} . Therefore the hole gas can be viewed as being confined in the effective thickness layer, and the dielectric constant can be seen as the same at the proximity of the effective boundary.

3.3.1 Solving to obtain induced potential

We used the finite-difference approximation [55] to discretize Eq. (3.10) in the form of a sparse matrix, which was solved using mixed boundary conditions. Two matrices were employed on each side of the interface. Mixed boundary conditions were applied to both sides, and a random value dif assigned to be the gradient of the left side; then the gradient of the right one would be 5.5 times of the random value. The solution was found when the value at the interface given by both equations agreed.

On the left side of the interface:

$$\begin{aligned} & \begin{bmatrix} -2 - step^2 \cdot q^2 & 1 & & \\ 1 & & \dots & \\ & & \dots & \dots & 1 \\ & & & 1 & -1 - step^2 \cdot q^2 \end{bmatrix} \cdot \begin{bmatrix} I(1) \\ \dots \\ \dots \\ I(N) \end{bmatrix} \\ &= \begin{bmatrix} step^2 \cdot \zeta_1^2(1) \\ \dots \\ \dots \\ step^2 \cdot \zeta_1^2(N) - dif \cdot step \end{bmatrix} \end{aligned} \quad (3.12)$$

On the right side of the interface:

$$\begin{aligned}
& \begin{bmatrix} -1 - \text{step}^2 \cdot q^2 & 1 & & \\ 1 & & \dots & \\ & & \dots & 1 \\ & & 1 & -1 - \text{step}^2 \cdot q^2 \end{bmatrix} \cdot \begin{bmatrix} I(N+1) \\ \dots \\ \dots \\ I(2N) \end{bmatrix} \\
& = \begin{bmatrix} 5.5 \cdot \text{dif} \cdot \text{step} \\ \dots \\ \dots \\ 0 - \text{dif} \cdot \text{step} \end{bmatrix}
\end{aligned} \tag{3.13}$$

where step is the step length we adopted for discretizing the space.

Once the induced potential is obtained, the dielectric function is at our disposal for the derivation of the dispersion relation.

The relationship between induced potential and total potential is

$$\langle l''' | V_q^s(z) | l'' \rangle = \sum_{kl, \frac{k+l}{2} = l'} \chi_{l' l'' l'''} \langle k' l' | V(r_{\parallel}, z) | kl \rangle \delta_{k', k+q} \tag{3.14}$$

where $|l\rangle$ is the wave function in z direction with subband number l .

The polarization term is given by

$$\chi_{l' l'' l'''} = \frac{2e^2}{\epsilon \epsilon_0 A} \frac{f_0(E_{k'l'}) - f_0(E_{kl})}{E_{k'l'} - E_{kl} + \hbar\omega - i\hbar\delta} R_{l' l'' l'''} \tag{3.15}$$

Since the total potential is the sum of the induced potential V_s and the external potential V_0 , the expectation value of V_0 is

$$\begin{aligned}
\langle k' l' | V_0 | kl \rangle &= \langle l' | V_{q0}(z) | l \rangle \\
&= \sum_{l'', \frac{l+l''}{2} = l'} \left(\delta_{ll''} \delta_{l'l''} - \sum_k \chi_{l' l'' l'''} \right) \times \langle l''' | V_q(z) | l'' \rangle
\end{aligned} \tag{3.16}$$

The quantity in the bracket of Eq. (3.16) is the dielectric function

$$\epsilon_{l' l'' l'''} = \delta_{ll''} \delta_{l'l''} - \sum_k \chi_{l' l'' l'''} \tag{3.17}$$

3.3.2 Dispersion relation of the collective excitation of a Q2D system

The intra-band term within ground state can be written as

$$R_{1111} = \int dz I(z) \zeta_1^2(z) \quad (3.18)$$

Therefore the dielectric function reduces to

$$\varepsilon_{1111} = 1 - \sum_k \frac{2e^2}{\varepsilon\varepsilon_0 A} \frac{f_0(E_{k,1}) - f_0(E_{k,1})}{E_{k,1} - E_{k,1} + \hbar\omega - i\hbar\delta} R_{1111}(q) \quad (3.19)$$

Given the explicit expression for 2D permittivity and the zeros of the dielectric function [33], one can get the dispersion relation for the Q2D case

$$\omega^2 = \left(\frac{2\pi n\hbar}{m_{\perp}^* m_e} \right)^2 \frac{1}{2B} \frac{q}{q_f} \cdot \frac{\left(1 + B \frac{q}{q_f} \right)^2 \left[1 + \frac{1}{2} B \left(\frac{q}{q_f} \right)^2 + \frac{1}{4} B^2 \left(\frac{q}{q_f} \right)^4 \right]}{\left(1 + \frac{1}{2} B \frac{q}{q_f} \right)} \quad (3.20)$$

where $\frac{\hbar^2 k_f}{2m_{\perp}^*} = \sqrt{2\pi n}$ is the Fermi wave number, and $B = \frac{\hbar^2 k_f^2 \varepsilon\varepsilon_0}{4m_{\perp}^* m_e e^2 q R_{1111}(q)}$.

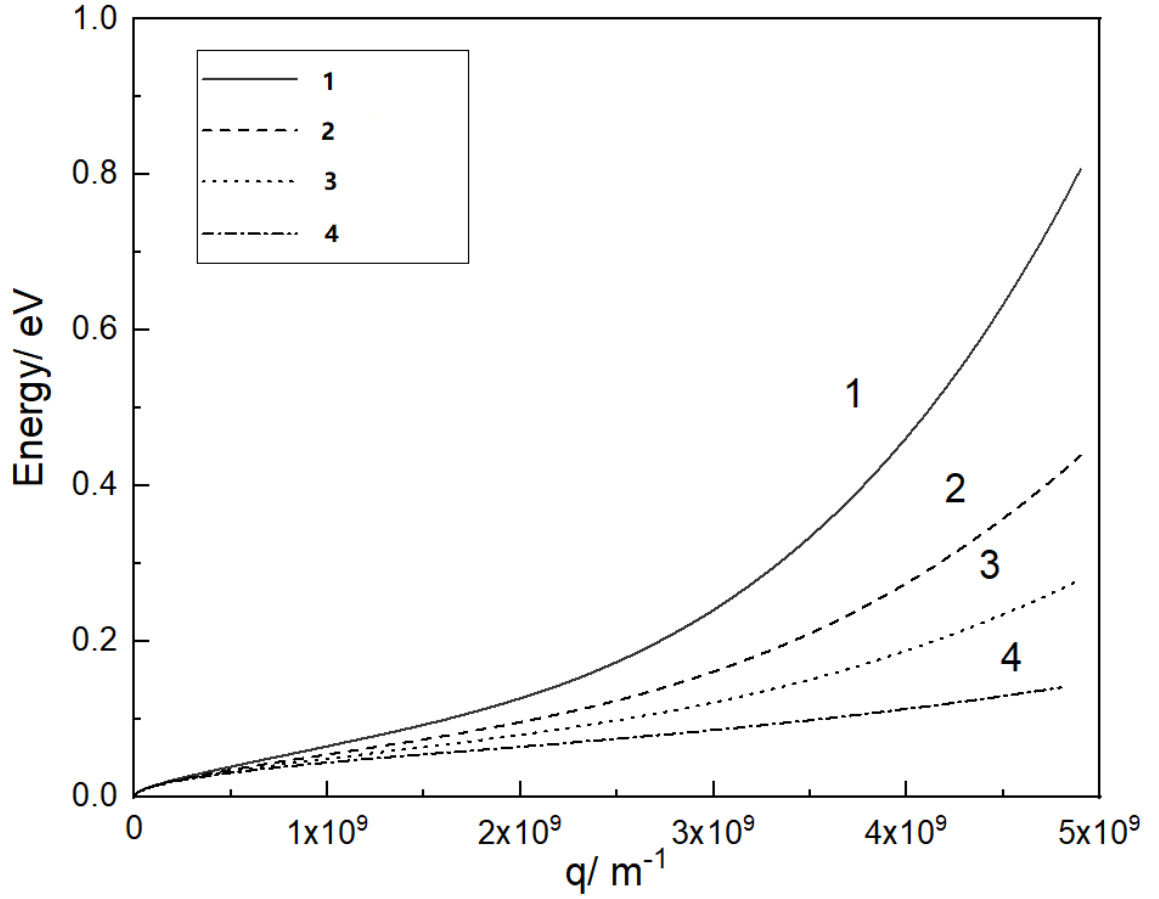


Figure 3.3: Plasmon dispersion relation for 2D and Q2D systems of different effective electric strength. Line 1 is the dispersion relation of Q2D system without external electric field, 2 and 3 are the dispersion relation of a Q2D system with effective electric strength equal to $10F$ and $100F$. Line 4 is the dispersion relation of a 2D system.

The plasmon dispersion relation $E(q)$ of 2D and Q2D system is plotted in Fig. (3.3). The energy E is proportional to the square root of the wavenumber for small wavenumbers, the square of wavenumber for $q \geq 10^9 m^{-1}$. This gives insight to locate the appropriate wavelength range to excite plasmons in the Q2D system. Applying an external electric field to the system ‘squeezes’ the conducting layer; for sufficiently high fields the system can be viewed as the pure 2D case. In Fig. (3.3), the effective electric field strength is modulated from $10F$ to $100F$, one can find that the plasmon dispersion relation is getting closer to that of pure 2D case, which validates that pure 2D case can be viewed as one particular condition of our Q2D method when effective electric field strength becomes infinitely large. For the low wavenumber limit, there is little variation in the dispersion relation with applied

fields, and the 2D and Q2D cases nearly coincide.

The appropriate wavelength of light to excite plasmons in the Q2D can be obtained by locating the point at which the plasmon and photon dispersion relations are equal. This is done in Fig. (3.4). The crossing point is $q = 50 \text{ m}^{-1}$, corresponding to radio waves of a wavelength of 12.6 cm or frequency of 2.4 GHz .

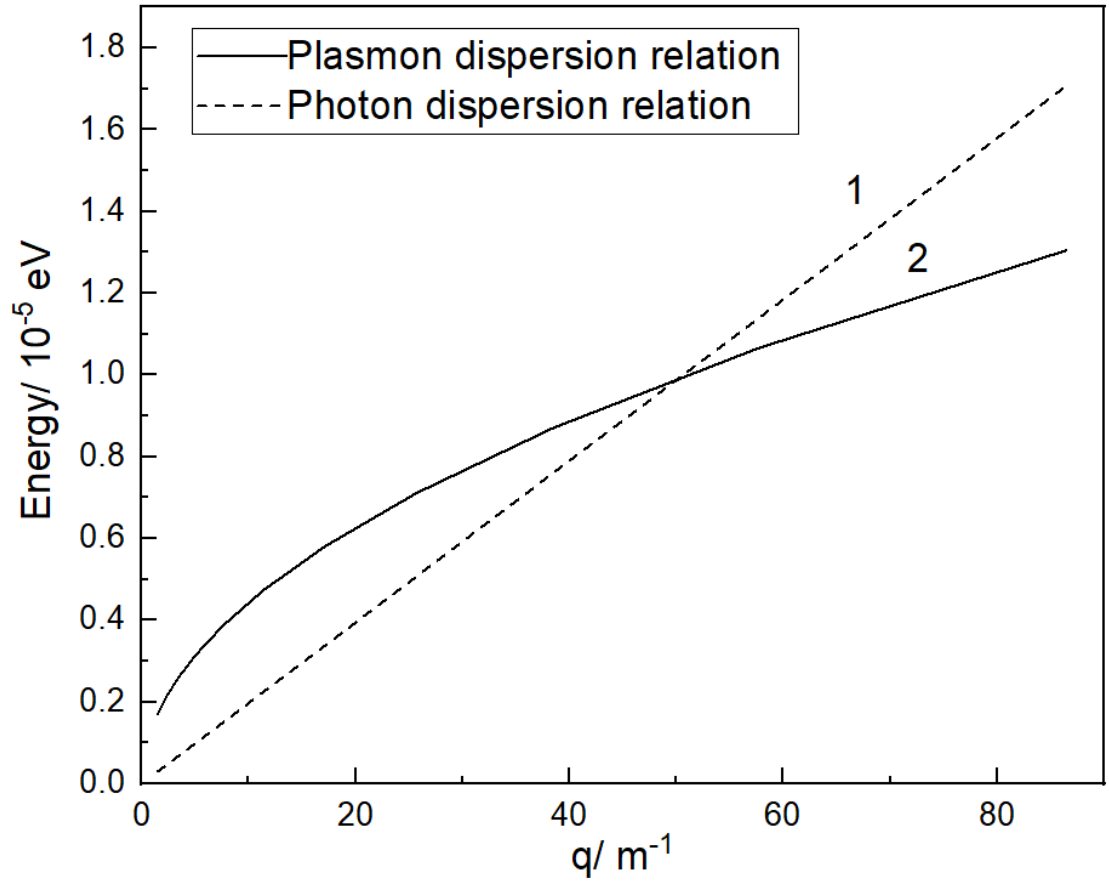


Figure 3.4: Dispersion relation for photon and Q2D system without external electric field. Line 1 is the dispersion relation of a photon, line 2 is the plasmon dispersion relation of a Q2D system.

3.3.3 Comparison of static dielectric function between Q2D and 2D system

For the general case, by denoting form factor $\gamma(q) = qR_1(q)(\varepsilon + 1)/\varepsilon$, we can write the dielectric function in the form

$$\varepsilon_{11,11} = 1 - \gamma(q)Q_0^{2D}(q) \quad (3.21)$$

where $Q_0^{2D}(q)$ is the polarizability of a two-dimensional non-interacting electron gas given by

$$Q_0^{2D}(q) = \sum_k \frac{4e^2}{(\varepsilon + 1)\varepsilon_0 A q} \frac{f_0(E_{k'}) - f_0(E_k)}{E_{k'} - E_k + \hbar\omega - i\hbar\delta} \quad (3.22)$$

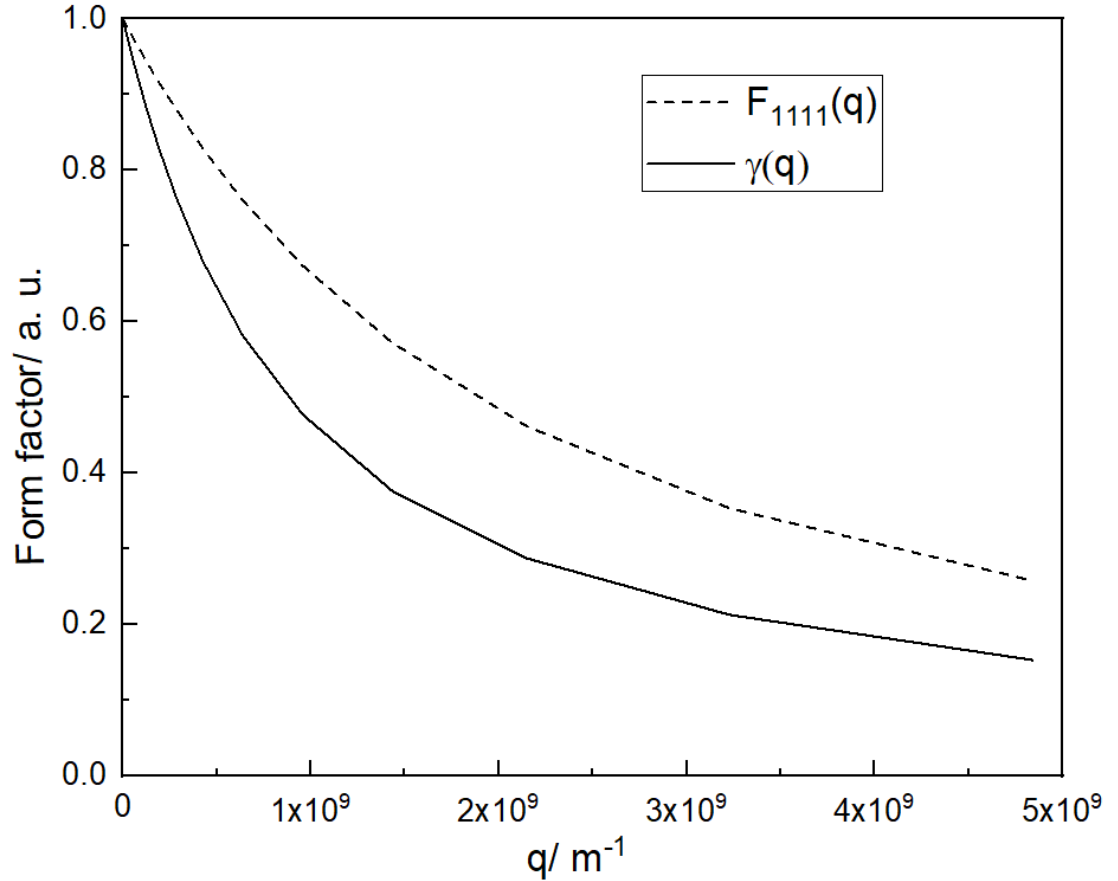


Figure 3.5: Form factor γ and F_{1111} as a function of q for the case where the surrounding media is vacuum.

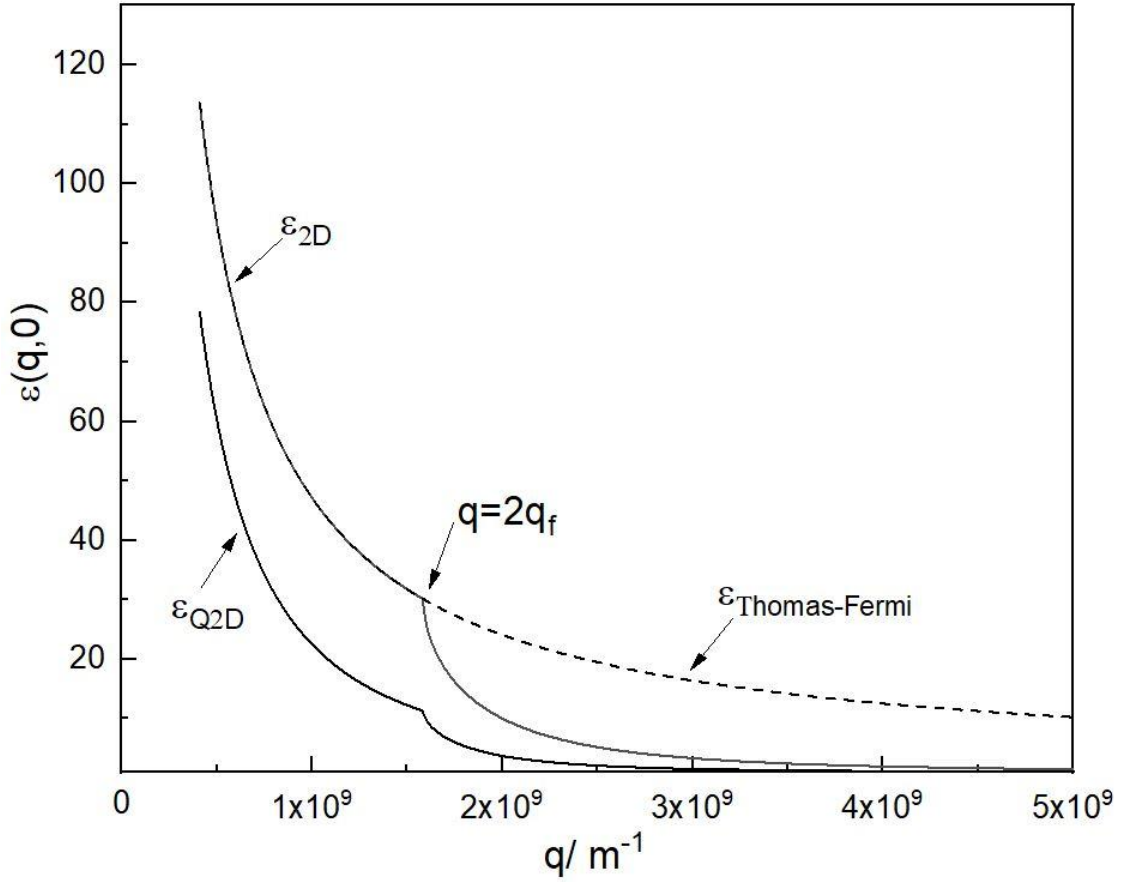


Figure 3.6: Static dielectric function is shown as a function for Q2D and 2D systems and also for Thomas-Fermi approximation.

Mori et. al. [56] use F_{ijkl} to denote the difference between 2D and Q2D systems, where the subscript labels the subband number along the z direction. It can be considered as the special case to our method that the conductive layer is embedded in the dielectric medium with the same dielectric constant as the conductive layer. Then the solution to the equation in the Sec. 3.1 can be written as

$$I(z) = \frac{2}{q} \int dz' e^{-q|z-z'|} \zeta_1^2(z') \quad (3.23)$$

Then the form factor for the intra-subband transition in the ground state is written as

$$F_{1111} = \int \int dz dz' \zeta_1^2(z) e^{-q|z-z'|} \zeta_1^2(z') \quad (3.24)$$

As one can easily tell from Fig. (3.5), the difference with and without continuity condition is not negligible. Also, one can find that γ and F_{1111} reduces to unity while q approaches

0, and the dielectric function for a Q2D system reduces to that for a 2D system as expected. γ drops sharply when q increases, showing that there is a significant difference between a 2D and a Q2D system in terms of dielectric function. To examine the deviation of the static dielectric function between Q2D and 2D system, we use an analytic form [57] for it when the hole gas is completely degenerated and obtain:

$$\begin{aligned} \epsilon^{Q2D}(q, 0) &= \begin{cases} 1 + \left(\frac{2}{qa^*} \right) \gamma(q), & q \leq 2q_F \\ 1 + \left(\frac{2}{qa^*} \right) \gamma(q) \cdot \left\{ 1 - \left[1 - \left(\frac{2q_F}{q} \right)^2 \right]^{\frac{1}{2}} \right\}, & q > 2q_F \end{cases} \end{aligned} \quad (3.25)$$

where $a^* = \epsilon_b \hbar^2 / m^* e^2$ is the effective Bohr radius. These are plotted in Fig. (3.6), and there is a noticeable difference between the dielectric function in the 2D and Q2D cases. This indicates that using the 2D case overestimates the screening effect of the charge carriers. The sharp drop when $q = 2q_f$ is called the Kohn effect [57], and arises from the singularity of the dielectric function. The 2D dielectric function using the Thomas-Fermi approximation is plotted in Fig. (3.5) as well, and we see that it is only valid for $q < 2q_f$.

3.3.4 Conclusions

In deriving the dielectric function of a Q2D material, we have constructed the relationship between induced and total potential by means of a Poisson equation [31], which naturally introduces the continuity conditions, making it an overall more accurate model. We also considered the triangular potential for a more realistic representation of a Q2D system in the 2DHG confined on the hydrogen terminated diamond. We have found that in the dispersion relation of a Q2D system, plasmon energy is proportional to the square root of the wavenumber for small wavenumber (q), and is proportional to the square of the wavenumber when the wavenumber (q) exceeds $10^9 m^{-1}$. The appropriate frequency of a photon able to excite longitudinal plasmon is around $2.4 GHz$, which is around 3 magnitudes lower than that of graphene plasmon [40,41]. By applying an external electric

field to the Q2D system, it is shown that the plasmon dispersion can be tuned to be close to that of the 2D case. We also compared the static function of Q2D system with the pure 2D one and found that the 2D results would overestimate the screening effect, making the Kohn effect less prominent in the Q2D case. We hope that our results will be useful in giving an insight into the exciting potential of light-carrier interactions in 2DHG supported by the hydrogen-terminated diamond, which may then be useful in exploring diamond-based plasmonic optoelectronic devices.

4

Future work

4.1 Introduction

The main result of a theoretical model has been completed in the previous chapter to obtain the dielectric function with triangular potential well in the z direction of a Q2D system. The following pilot studies have been done to probe more into the practical aspects of obtaining the dielectric function of hydrogen terminated diamond. These include photocurrent and ellipsometry measurements. These results are not conclusive but will constitute as future work given more time and resources.

4.2 Measurement of photoconductivity of hydrogen-terminated diamond

The interaction of photon and charge carriers in an electronic system is not limited to SPP. Another pathway is the photoconductivity in the condensed matter system. Photocurrent occurs in a semiconductor when the photon energy of incident light is equal or higher than the band gap, leading to the creation of photo-induced charge carriers in the conduction band and valence band [58]. Hydrogen-terminated Diamond is known to exhibit photoconductivity in the ultraviolet regime ($E_g=5.47$ eV) however there have been emerging reports on the sub-band-gap excitation induced photoconductivity. The mechanism behind it still remains controversial, for example whether this property comes from the bulk diamond (with defects) or the 2D hole conducting layer [59].

To explore the photoconductivity properties of surface conducting hydrogen-terminated diamond, we made four devices on one diamond sample which includes 2 kinds of channel dimensions multiplied by two regions which are hydrogenated and oxygenated respectively. Our research interest lies in the hydrogenated region which is conductive while the oxygenated region is insulating.

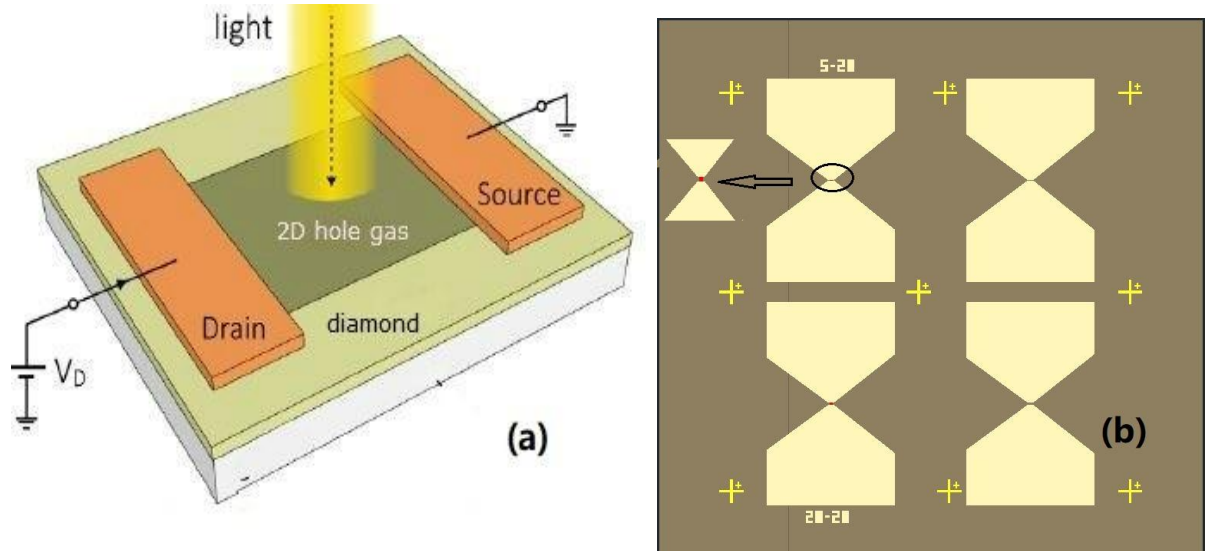


Figure 4.1: (a) Schematic image of the device design for photocurrent measurement; (b) the images of the four devices under optical microscopy. The left two devices are hydrogen terminated areas, while the right two are the oxygen terminated. The channel dimension (red region) is $5\mu m \times 20\mu m$ and $20\mu m \times 20\mu m$.

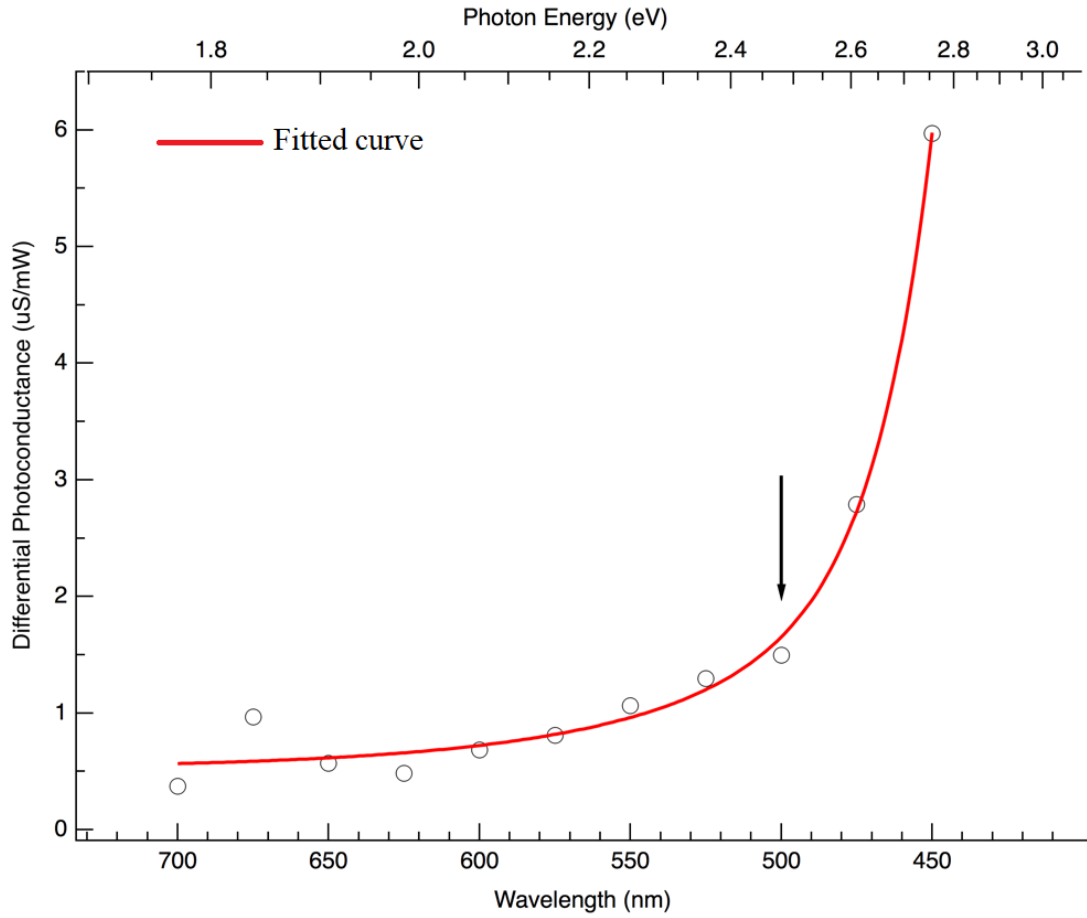


Figure 4.2: The relation between photoconductance and wavelength in the hydrogenated area.

The light source we used here was Fianium SC-450-2, which can modulate the wavelength through a wide range. The photocurrent has been normalised to the illumination power of the laser at each wavelength. We can tell from the plot that photoconductance increased dramatically from 500 nm , which indicates that the on-set of photocurrent generation is at 500 nm . The photon energy is much smaller than the band gap of a diamond, which might result from the defect in the surface that helps narrow the band gap.

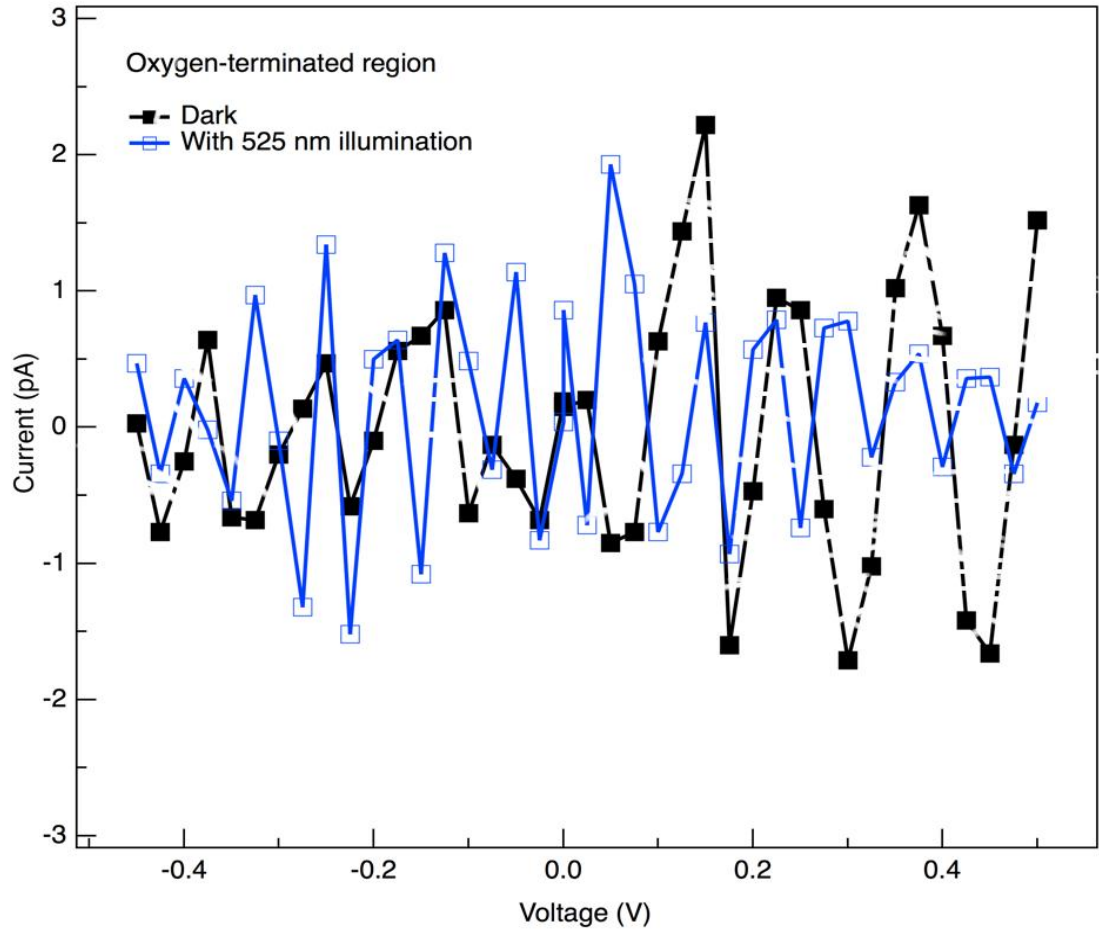


Figure 4.3 The comparison of I-V measurements in dark and with 525 *nm* laser illumination for oxygen-terminated channel.

We want to show that the photoconductivity is related with the occurrence of a 2D hole gas, thus we draw the IV curve with and without light illumination in the oxygenated area (Fig. (4.3)). One can tell from the plot that the current with or without the laser illumination are both within noise level, which suggests that photoconductivity is not a bulk phenomenon, instead it's closely related to the 2D hole gas. The wavelength relevant to photoconductivity occurs in 500 *nm* visible light regime, while for most other 2D materials plasmonic excitation occurs in far-infrared or even terahertz regimes given the much lower carrier density compared to metal. In conclusion the result shows that carrier concentration won't be changed at the wavelengths relevant to exciting SPP because photocurrent and SPP occurring very distinct spectrums. For future work, it's worth investigating whether SPP can be coupled to the photocurrent effect, via tuning the plasmonic response of the diamond by terahertz or far-infrared light.

4.3 Ellipsometry measurements

It is feasible to measure the dielectric function using ellipsometry [60], which can directly relate to the theoretical results from Chapter 3, therefore paving the way to the plasmonic realization ultimately. We hope this study lays an important foundation towards any future work of investigation into the optical properties of such 2DHG systems.

Dielectric function is the key parameter in determining the optical properties, so the measurement of dielectric function was also conducted using J.A. Woollam IR-VASE Infrared variable angle spectroscopic ellipsometer at the University of Adelaide.

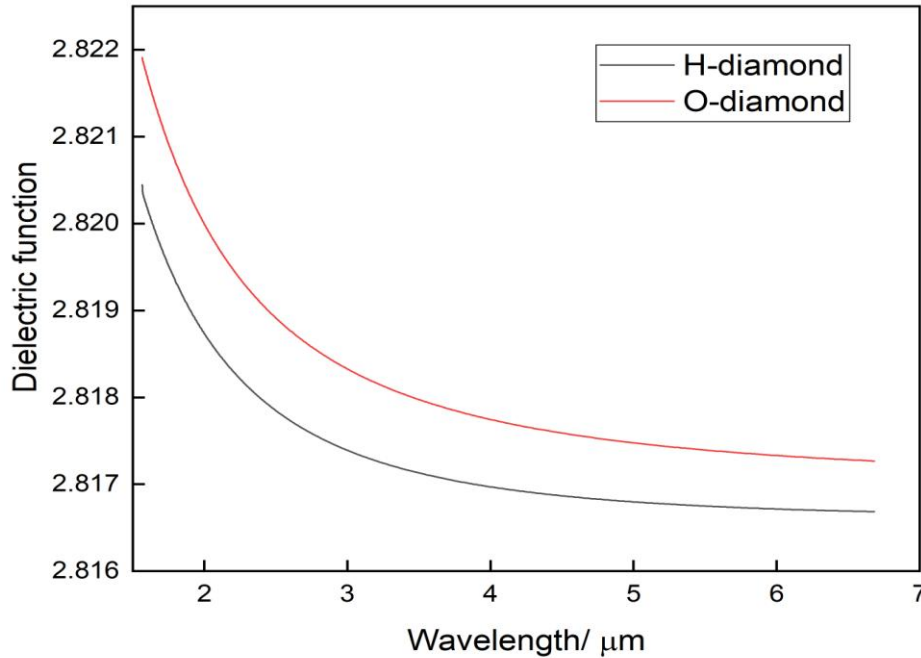


Figure 4.4: Dielectric function of hydrogen and oxygen terminated diamond in the infrared range.

The data of the hydrogen terminated diamond and the oxygen terminated diamond were fit (with angle offset increasing RI) using a Cauchy model Angle offset. Regardless, the fact that the reference and H-terminated diamond differ only slightly (Fig. (4.4)) indicates no large absorption in this wavelength range.

Because the back reflection from a thick diamond substrate is very weak, which means there could be lots of noise in the signal. One way to verify whether the slight difference arises from the thin layer of 2D hole gas or not is to form a 2D hole gas on a much thinner diamond substrate, say 100 nm thickness, which will be able to generate higher signal to noise ratio. Once the work of cross checking theoretically and experimentally on the optical parameters of hydrogen terminated diamond is done, plasmonic devices can be designed using simulation software such as Lumerical FDTD.

Once we can simulate various designs of the plasmonic interactions on hydrogen-terminated diamond, it is possible to tune its dispersion relation via changing the carrier density. This has the added advantage of overcoming the hurdle of significant propagating loss suffered by SPP. With a potential design, the realization of plasmonic excitation on the diamond surface can be deployed with SNOM probing on the device fabricated with the parameters obtained from simulation. The extraordinary properties of such device await to be explored.

4.4 Refinement on theoretical analysis

Based on the same theoretical framework done by Ehrenreich [29], A. Hill *et. al.* [61] studied the dielectric function and plasmonic properties using the Bloch wave function from the tight-binding approximation, in which the Brillouin zone is indicated by the hexagon which connects the Dirac nodes, thus generating a linear band structure. Whereas in our case we adopted the free electron/hole wave function, hence the band structure is parabolic shaped. In the long wavelength limit, the plasmon energy of graphene is still proportional to the square root of wavenumber, but not the square root of charge carrier density in the parabolic band structure approximation, instead it's proportional to the quartic root of the charge carrier density. This inspire us to consider the light hole, heavy hole and split off band structure in the case of hydrogen terminated diamond surface, and use the Bloch wave function instead of free charge carrier wave function. Though our approximation well describes the situation in which heavy hole band is mostly populated on the diamond surface, the consideration of other two bands will increase the accuracy of the analysis.

Also DFT (Density functional theory) calculation has been widely used for accurate analysis of plasmonic properties, in which the cell structure, doping material and other parameters

are all accounted for [62]. The previous method is based on random phase approximation to deal with many body interaction, specifically the coulomb interaction when analyzing plasmonic /collective excitation. Whereas for DFT calculation, the interaction effect exerted on each of every particle is studied separately, which can only be done with massive computation resources. Recently a new technique for quasi-low-dimensional DFT is developed by Vladimir U. Nazarov [51], who proposed that the energy split due to vertical confinement can be included during calculation.

Experiment wise, D. N. Basov *et. al.* [62] summarized all kinds of two-dimensional polariton, including SSP, phonon polariton, exciton polariton, etc., within the framework of semi-classical model of conductivity, which is written as following

$$\sigma(\omega) = \frac{i}{\pi} \frac{S_f}{\omega + i\tau_f^{-1}} + \frac{i}{\pi} \frac{S_b}{\omega^2 - \omega_b^2 + i\omega\tau_f^{-1}} \quad (4.1)$$

The first and second term stands for the contribution from free (f) and bound (b) charges, and ω_b is the phonon frequency, and S_f , S_b , τ_f are the quantities given by experimental measurement. Here we notice that our case matches well with the conductivity when only free charges term is considered as in Eq. (2.18) and (2.19). This motivates us to experimentally realize the plasmonic excitation using hydrogen terminated diamond, to figure out the novel phenomenon beyond the simplified theoretical model.

5

Summary and Conclusion

This thesis focuses on the plasmonic excitation of Q2D materials theoretically. In particular the 2DHG on diamond was analyzed as a particular example. In the literature review the definition of plasmons are discussed thoroughly, and different models to derive the plasmonic dispersion relation are given, in which the self-consistent field approach is discussed in detail. In the Chapter 3 the main result of the dielectric function for the 2DHG system was presented by extending the published work of Lee [31], changing the confining potential to a triangular well which better approximates the confining potential profile at diamond surface as well as in other semiconductor heterostructures. Later the plasmon dispersion relation is discussed with this newly proposed mathematical framework and it is found that the plasmon energy is proportional to the square root of wavenumber for small wavenumber, and the square of wavenumber when wavenumber exceeds 10^9 m^{-1} . This leads to the key result of the light momentum matching condition at wavenumber of 50 m^{-1} . This means that if a plasmon is supported in the 2DHG for hydrogen-terminated diamond, it will be around the GHz range. The theoretical framework developed in this work in obtaining the dielectric function for a Q2D system with a non-square confining potential will not only guide future experimental work in this field, but also lay a foundation to model the realistic dielectric functions in other types of promising 2D or Q2D materials.

The pilot studies of photocurrent and ellipsometry were also conducted on hydrogen terminated diamond. It is found that the wavelength relevant to photoconductivity occurs in the 500 nm visible light regime, and there is slight difference between the dielectric functions of hydrogen and oxygen terminated diamond in the far-infrared range. Future work can be done on verifying whether plasmonic response of the diamond by terahertz or far-infrared light can be coupled to the photocurrent effect, and whether forming 2D hole gas on a much thinner diamond substrate would give us different results through higher signal to noise ratio.

References

- [1] Born, Max, and Emil Wolf. Principles of optics: electromagnetic theory of propagation, interference and diffraction of light. Elsevier, 2013.
- [2] Hecht, Bert, et al. "Scanning near-field optical microscopy with aperture probes: Fundamentals and applications." The Journal of Chemical Physics 112.18 (2000): 7761-7774.
- [3] Dongzhi Chi, K.E. Johnson Goh, Andrew T.S Wee, eds. 2D Semiconductor Materials and Devices. Elsevier, 2019.
- [4] Kawarada, Hiroshi. "Hydrogen-terminated diamond surfaces and interfaces." Surface Science Reports 26.7 (1996): 205-259.
- [5] Zenneck, Jonathan. "Über die Fortpflanzung ebener elektromagnetischer Wellen längs einer ebenen Leiterfläche und ihre Beziehung zur drahtlosen Telegraphie." Annalen der Physik 328.10 (1907): 846-866.
- [6] Sommerfeld, Arnold. "Über die Ausbreitung der Wellen in der drahtlosen Telegraphie." Annalen der Physik 333.4 (1909): 665-736.
- [7] Tolpygo, K. B. "Physical properties of a rock salt lattice made up of deformable ions." Ukr. J. Phys 53 (2008): 93-102
- [8] Huang, Kun. "Lattice vibrations and optical waves in ionic crystals." Nature 167.4254 (1951): 779.
- [9] Hopfield, J. J. "Theory of the contribution of excitons to the complex dielectric constant of crystals." Physical Review 112.5 (1958): 1555.
- [10] Bohm, David, et al. "A collective description of electron interactions: III. Coulomb interactions in a degenerate electron gas." Physical Review 92.3 (1953): 609.
- [11] Frohlich, H., et al. "Plasma oscillations and energy loss of charged particles in solids." Proceedings of the Physical Society. Section A 68.6 (1955): 525.
- [12] Ritchie, R. H. "Plasma losses by fast electrons in thin films." Physical Review 106.5 (1957): 874.
- [13] Otto, Andreas. "Excitation of nonradiative surface plasma waves in silver by the method of frustrated total reflection." Zeitschrift für Physik A Hadrons and nuclei 216.4 (1968): 398-410.

- [14] Maier, Stefan Alexander. Plasmonics: fundamentals and applications. Springer Science & Business Media, 2007.
- [15] Wang, Y., et al. "Foundations of plasmonics." *Advances in Physics* 60.5 (2011): 799-898.
- [16] Yoon, Hosang. Two-Dimensional Plasmonics in Massive and Massless Electron Gases. Diss. Harvard University, 2014.
- [17] Kretschmann, Erwin, et al. "Radiative decay of non radiative surface plasmons excited by light." *Zeitschrift fur Naturforschung A* 23.12 (1968): 2135-2136.
- [18] Ajayan, Pulickel, Philip Kim, and Kaustav Banerjee. "van der Waals materials." *Physics Today* 69 (2016): 9-38.
- [19] Xu, Mingsheng, et al. "Graphene-like two-dimensional materials." *Chemical reviews* 113.5 (2013): 3766-3798.
- [20] Zhi, Chunyi, et al. "Boron nitride nanotubes/polystyrene composites." *Journal of Materials Research* 21.11 (2006): 2794-2800.
- [21] Butler, Sheneve Z., et al. "Progress, challenges, and opportunities in two-dimensional materials beyond graphene." *ACS nano* 7.4 (2013): 2898-2926.
- [22] Kooi, Bart J., et al. "Ferroelectric chalcogenides materials at the edge." *Science* 353.6296 (2016): 221-222.
- [23] Xie, L. M. "Two-dimensional transition metal dichalcogenide alloys: preparation, characterization and applications." *Nanoscale* 7.44 (2015): 18392-18401.
- [24] Fal'Ko, V. I., et al. "What if a film conductivity exceeds the speed of light?." *Zh. Eksp. Teor. Fiz* 95 (1989): 1988-1992.
- [25] Jablan, Marinko, et al. "Plasmonics in graphene at infrared frequencies." *Physical review B* 80.24 (2009): 245435.
- [26] Stern, Frank. "Polarizability of a two-dimensional electron gas." *Physical Review Letters* 18.14 (1967): 546.
- [27] Ukhtary, Muhammad Shoufie. "Surface electromagnetic wave in two-dimensional materials." (2018).
- [28] Xia, Fengnian, et al. "Two-dimensional material nanophotonics." *Nature Photonics* 8.12 (2014): 899.

- [29] Ehrenreich, H., et al. "Self-consistent field approach to the many-electron problem." *Physical Review* 115.4 (1959): 786.
- [30] Wooten, Frederick. *Optical properties of solids*. Academic press, 2013.
- [31] Lee, Johnson, et al. "Dielectric function for a quasi-two-dimensional semiconducting system." *Journal of applied physics* 54.12 (1983): 6989-6994.
- [32] Khanh, Nguyen Quoc. "Dielectric function and plasmon dispersion relation of a quasi-two-dimensional electron gas." *physica status solidi (b)* 197.1 (1996): 73-79.
- [33] Czachor, A., et al. "Dynamical correlations in a two-dimensional electron gas: First-order perturbation theory." *Physical Review B* 25.4 (1982): 2144.
- [34] Aharonyan, K. H. "Dielectric function and collective plasmon modes of a quasi-two-dimensional finite confining potential semiconductor quantum well." *Physica E: Low-dimensional Systems and Nanostructures* 43.9 (2011): 1618-1624.
- [35] <https://www.jawoollam.com/resources/ellipsometry-tutorial/what-is-ellipsometry>.
- [36] Goldstein, Joseph I., et al. *Scanning electron microscopy and X-ray microanalysis*. Springer, 2017.
- [37] Reimer, Ludwig. *Transmission electron microscopy: physics of image formation and microanalysis*. Vol. 36. Springer, 2013.
- [38] Chen, C. Julian. *Introduction to scanning tunneling microscopy*. Vol. 4. Oxford University Press on Demand, 1993.
- [39] <https://www.manualslib.com/products/Nt-Mdt-Ntegra-Spectra-Probe-Nanolaboratory-10228573.html>
- [40] Chen, Jianing, et al. "Optical nano-imaging of gate-tunable graphene plasmons." *Nature* 487.7405 (2012): 77.
- [41] Fei, Zhe, et al. "Gate-tuning of graphene plasmons revealed by infrared nano-imaging." *Nature* 487.7405 (2012): 82.
- [42] Zayats, et al. (2005). *Nano-optics of Surface Plasmon Polaritons*. *Physics reports*, 408(3), 131-314.
- [43] Basov, D. N., et al. "Polaritons in van der Waals materials." *Science* 354.6309 (2016): aag1992
- [44] Weisbuch, Claude, and Borge Vinter. *Quantum semiconductor structures: fundamentals and applications*. Elsevier, 2014.

- [45] Fetter, Alexander L. "Electrodynamics of a layered electron gas. I. Single layer." *Annals of Physics* 81.2 (1973): 367-393.
- [46] Fetter, Alexander L. "Electrodynamics of a layered electron gas. II. Periodic array." *Annals of Physics* 88.1 (1974): 1-25.
- [47] Volkov, V. A., and Sergey A. Mikhailov. "Edge magnetoplasmons: low frequency weakly damped excitations in inhomogeneous two-dimensional electron systems." *Sov. Phys. JETP* 67.8 (1988): 1639-1653.
- [48] Backes, W. H., et al. "Dispersion of longitudinal plasmons for a quasi-two-dimensional electron gas." *Physical Review B* 45.15 (1992): 8437.
- [49] Bazhenov, N. L., K. D. Mynbaev, and G. G. Zegrya. "Dielectric function of quasi-2D semiconductor nanostructures." *Semiconductors* 41.2 (2007): 184-189.
- [50] Konar, Aniruddha, et al. "Dielectric-environment mediated quantum screening of two-dimensional electron gas." *Journal of Applied Physics* 114.11 (2013): 113707.
- [51] Nazarov, Vladimir U. "Quasi-Low-Dimensional Electron Gas with One Populated Band as a Testing Ground for Time-Dependent Density-Functional Theory of Mesoscopic Systems." *Physical review letters* 118.23 (2017): 236802.
- [52] Maier, F., et al. "Origin of surface conductivity in diamond." *Physical review letters* 85.16 (2000): 3472.
- [53] Sussmann, Ricardo S., ed. *CVD diamond for electronic devices and sensors*. Vol. 26. John Wiley & Sons, 2009.
- [54] Gan, L., et al. "Quantization of 2D hole gas in conductive hydrogenated diamond surfaces observed by electron field emission." *Physical review letters* 96.19 (2006): 196808.
- [55] J. W. Thomas, *Numerical Partial Differential Equations: Finite Difference Methods*, first ed., Springer, New York, 1995.
- [56] Mori, Shojiro, and Tsuneya Ando. "Electronic properties of a semiconductor superlattice II. Low temperature mobility perpendicular to the superlattice." *Journal of the Physical Society of Japan* 48.3 (1980): 865-873.
- [57] Mahan, Gerald D. *Many-particle physics*. Springer Science & Business Media, 2013.
- [58] Mort, Joseph, and Damodar Mangalore Pai. *Photoconductivity and related phenomena*. distributors for the US and Canada, Elsevier/North-Holland, 1976.
- [59] Williams, Oliver A., and Richard B. Jackman. "Surface conductivity on hydrogen terminated diamond." *Semiconductor science and technology* 18.3 (2003): S34.

- [60] Cushman, Cody V., et al. "An Introduction to Modeling in Spectroscopic Ellipsometry, Focusing on Models for Transparent Materials: the Cauchy and Sellmeier Models."
- [61] Hill, Antonio, Sergey A. Mikhailov, and Klaus Ziegler. "Dielectric function and plasmons in graphene." *EPL (Europhysics Letters)* 87.2 (2009): 27005.
- [62] Torbatian, Zahra, and Reza Asgari. "Plasmonic physics of 2D crystalline materials." *Applied Sciences* 8.2 (2018): 238.
- [63] Basov, D. N., M. M. Fogler, and FJ Garc ía De Abajo. "Polaritons in van der Waals materials." *Science* 354.6309 (2016).